



Article

Inhibition of ATR Reverses a Mitochondrial Respiratory Insufficiency

Megan B. Borror^{1,2}, Milena Girotti^{1,2}, Adwitiya Kar^{1,2}, Meghan K. Cain^{1,2}, Xiaoli Gao³, Vivian L. MacKay⁴, Brent Herron⁵, Shylesh Bhaskaran^{1,2}, Sandra Becerra^{1,2}, Nathan Novy⁶, Natascia Ventura^{7,8} , Thomas E. Johnson⁵, Brian K. Kennedy^{4,9,10} and Shane L. Rea^{1,2,6,*} 

- ¹ The Barshop Institute for Longevity and Aging Studies, University of Texas Health Science Center at San Antonio, San Antonio, TX 78229, USA; mbborror@ollusa.edu (M.B.B.); girotti@uthscsa.edu (M.G.); adwitiya.kar@cuanschultz.edu (A.K.); meghankcain@gmail.com (M.K.C.); bhaskarans@omrf.org (S.B.); becerras81@gmail.com (S.B.)
- ² Department of Physiology, University of Texas Health Science Center at San Antonio, San Antonio, TX 78229, USA
- ³ Department of Biochemistry, University of Texas Health Science Center at San Antonio, San Antonio, TX 78229, USA; shellygao2010@gmail.com
- ⁴ Department of Biochemistry, University of Washington, Seattle, WA 98195, USA; mackvl47@gmail.com (V.L.M.); bkennedy@buckinstitute.org (B.K.K.)
- ⁵ Institute for Behavioral Genetics, Department of Integrative Physiology, University of Colorado Boulder, Boulder, CO 80309, USA; brent.x.herron@kp.org (B.H.); johnsont@colorado.edu (T.E.J.)
- ⁶ Department of Laboratory Medicine and Pathology, University of Washington, Seattle, WA 98195, USA; novyn@uw.edu
- ⁷ IUF—Leibniz Research Institute for Environmental Medicine, 103045 Düsseldorf, Germany; natascia.ventura@uni-duesseldorf.de
- ⁸ Institute for Clinical Chemistry and Laboratory Diagnostic, Medical Faculty of the Heinrich Heine University, 103045 Düsseldorf, Germany
- ⁹ Buck Institute for Research on Aging, Novato, CA 94945, USA
- ¹⁰ Departments of Biochemistry and Physiology, Yong Loo Lin School of Medicine, National University of Singapore, Singapore 117542, Singapore
- * Correspondence: shanerea@uw.edu



Citation: Borror, M.B.; Girotti, M.; Kar, A.; Cain, M.K.; Gao, X.; MacKay, V.L.; Herron, B.; Bhaskaran, S.; Becerra, S.; Novy, N.; et al. Inhibition of ATR Reverses a Mitochondrial Respiratory Insufficiency. *Cells* **2022**, *11*, 1731. <https://doi.org/10.3390/cells11111731>

Academic Editor: Albert Quintana

Received: 26 April 2022

Accepted: 21 May 2022

Published: 24 May 2022

Publisher's Note: MDPI stays neutral with regard to jurisdictional claims in published maps and institutional affiliations.



Copyright: © 2022 by the authors. Licensee MDPI, Basel, Switzerland. This article is an open access article distributed under the terms and conditions of the Creative Commons Attribution (CC BY) license (<https://creativecommons.org/licenses/by/4.0/>).

Abstract: Diseases that affect the mitochondrial electron transport chain (ETC) often manifest as threshold effect disorders, meaning patients only become symptomatic once a certain level of ETC dysfunction is reached. Cells can invoke mechanisms to circumvent reaching their critical ETC threshold, but it is an ongoing challenge to identify such processes. In the nematode *Caenorhabditis elegans*, severe reduction of mitochondrial ETC activity shortens life, but mild reduction actually extends it, providing an opportunity to identify threshold circumvention mechanisms. Here, we show that removal of ATL-1, but not ATM-1, worm orthologs of ATR and ATM, respectively, key nuclear DNA damage checkpoint proteins in human cells, unexpectedly lessens the severity of ETC dysfunction. Multiple genetic and biochemical tests show no evidence for increased mutation or DNA breakage in animals exposed to ETC disruption. Reduced ETC function instead alters nucleotide ratios within both the ribo- and deoxyribo-nucleotide pools, and causes stalling of RNA polymerase, which is also known to activate ATR. Unexpectedly, *atl-1* mutants confronted with mitochondrial ETC disruption maintain normal levels of oxygen consumption, and have an increased abundance of translating ribosomes. This suggests checkpoint signaling by ATL-1 normally dampens cytoplasmic translation. Taken together, our data suggest a model whereby ETC insufficiency in *C. elegans* results in nucleotide imbalances leading to the stalling of RNA polymerase, activation of ATL-1, dampening of global translation, and magnification of ETC dysfunction. The loss of ATL-1 effectively reverses the severity of ETC disruption so that animals become phenotypically closer to wild type.

Keywords: aging; ageing; checkpoint response; DNA damage response; DDR; MAK-1; MAK-2; MAPKAPs; Mit mutants; polysome profiling; retrograde response

1. Introduction

The essential nature of mitochondria is underscored by the devastating effects of inherited mitochondrial diseases, which afflict approximately one in 5000 children and almost always result in pathological shortening of life [1]. Because these organelles play central roles in many cellular processes, including energy production, nucleotide metabolism, and apoptotic signaling [2–4], their progressive, age-dependent reduction in function means almost all of us, at some time in life, will experience the negative consequences of mitochondrial dysfunction [5]. Indeed, a growing number of age-related ailments common to western societies are either associated with, or directly caused by, mitochondrial disruption [6,7].

In *Caenorhabditis elegans*, as in humans, mitochondrial dysfunction is threshold-dependent, that is, a critical level of electron transport chain (ETC) dysfunction must be reached before pathology is observed [8]. Nematodes with high levels of mitochondrial dysfunction exhibit shortened lifespan and reduced fitness, whereas worms with moderate levels of mitochondrial dysfunction display an extended lifespan [9]. This response is evolutionarily conserved from yeast to mammals, and understanding the molecular mechanisms regulating lifespan extension in worms in response to mild ETC disruption may provide insight into strategies that could be applied to help keep our own cells above their critical mitochondrial dysfunction threshold.

Reduced ETC activity disrupts many downstream cellular processes, and, as might be expected, cells have evolved a variety of sensors and strategies to counter progression toward their critical ETC threshold. Multiple signaling pathways, collectively called retrograde responses, are activated within cells and these, in turn, control expression of nuclear counter-measures [10]. For example, an increase in the unfolded protein load of the mitochondrial matrix re-directs the transcription factor ATFS-1 from the matrix to the nucleus where it stimulates expression of mitochondrial chaperones [11]. Other signals, such as changes in calcium concentration, activation of mitogen-activated protein kinases (MAPKs), and even knock-on changes in the cytoplasmic unfolded protein load also result in retrograde response activation [12–14]. Counter-measures that are activated by cells include increased mitochondrial biogenesis, elevated mitochondrial DNA (mtDNA) replication, increased mitophagy, activation of alternate pathways of energy production (such as glycolysis), and changes in the abundance and activity of respiratory complexes or their regulatory factors [8,15,16]. The complete network of pathways that detect and respond to mitochondrial stress is, however, far from being fully understood [15].

Previously, we described a phenomenon in worms in which the loss of CEP-1, a homolog of the human p53 checkpoint protein that recognizes identical DNA sequences and is the only p53 family member present in *C. elegans* [16], right-shifted the mitochondrial ETC threshold, effectively allowing animals to cope with a greater degree of mitochondrial ETC disruption, and consequently mitigating the lifespan-shortening effects of severe mitochondrial dysfunction [17]. This response was due to alterations in autophagy and lipid metabolism, both of which are regulated by CEP-1 [18]. In the current study, we examined the role of other checkpoint proteins in modulating the mitochondrial threshold effect of worms, since this is still a little-explored area of investigation.

Ataxia-telangiectasia-mutated (ATM) and ‘ATM- and *rad3*-related’ (ATR) are two well-studied members of the phosphoinositide 3-kinase-related kinase (PIKK) family of proteins that play essential roles in transducing checkpoint signaling during the DNA damage response (DDR) [19]. In humans, both proteins together directly phosphorylate over 900 sites on some 700 proteins, including p53 [20]. ATM and ATR differ in the lesions to which they are recruited, with ATM being recruited to dsDNA breaks, and ATR having a broader specificity underscored by the presence of ssDNA, including recessed dsDNA breaks and stalled replication forks [21]. Depending on the level of damage and success of repair, checkpoint activation can lead to pro-survival or pro-apoptotic mechanisms [22]. Recently, additional functions were ascribed to both ATM and ATR. For ATM, these involve regulation of a variety of processes, including insulin signaling,

the pentose phosphate pathway, and mitophagy [23–27]. Moreover, in yeast, ATM/Tel1p was found to act as a specific sensor of mitochondria-generated ROS [28,29]. ATR, on the other hand, was shown to be important in controlling an outer mitochondrial membrane (OMM)-localized apoptotic signal, autophagy, RNA polymerase activity, and chromatin condensation [28–32].

In this study, we uncover a new role for ATR in mitochondrial retrograde response signaling. Studying *atl-1(tm853)* loss-of-function mutants in *C. elegans*, we show that ATR/ATL-1 is activated when the mitochondrial ETC is impaired. We find no evidence for increased nuclear DNA damage under these conditions, yet a significant change in ribose- and deoxyribose nucleotide pools is observed. Consistent with ATL-1 activation being tied to this alteration, we find an elevation in R-loop formation in *atl-1(tm853)* mutants following exposure to ETC disruption. R-loop formation is indicative of RNA pol II stalling, a known mechanism of ATR activation in human cells. Unexpectedly, we find that mutant *atl-1(tm853)* worms have half the amount of mitochondrial DNA of wild type worms, yet they show no reduction in the amount of oxygen they consume, neither under control- or ETC-disrupting conditions. In determining the mechanism by which ATL-1 functions to regulate mitochondrial retrograde response signaling, we show that ATL-1 inhibits translation, potentially through ICD-1, a ribosomal exit-tunnel chaperone. Finally, in the process of studying *atl-1(tm853)* mutants, we have discovered several other DNA damage response proteins, including MAPKAP-2 and MAPKAP-3, that function downstream of mitochondrial ETC disruption. These findings underscore what appears to be an extensive role for the DDR network in mitochondrial retrograde response signaling.

2. Methods

A detailed description of all methods is provided in File S1.

2.1. Nematode Strains and Maintenance

Genotypic information for all strains used in this study is provided in Table S4. Lines were maintained at 20 °C on standard NGM agar plates seeded with *E. coli* (OP50) [33]. To control for possible untoward effects derived from the *nT1(IV;V)* chromosomal pair in maternally-rescued *atl-1(tm853)* mutants, all lines, including the wild type control, were moved into the *nT1(IV;V)* background, and then unbalanced F1 animals were freshly collected for each relevant experiment. Further details are provided in File S1.

2.2. Bacterial Feeding RNAi

All bacterial feeding RNAi constructs were designed in the pL4440 vector backbone and maintained in HT115 bacteria [34]. Growth rate, life span, RNAi efficacy assays, and RNAi dilution methods are described in File S1.

2.3. Microscopy

Images of fluorescent worms were captured using an Olympus SZX16 fluorescence microscope connected to an Olympus DP71 CCD camera. In Figure 7C, to determine whether differences existed in the morphology of mitochondria between the four tested conditions, four randomly selected images from each condition were mixed and then grouped by a scorer who was blind to image identity. In a set of 16 images, 10 were co-grouped correctly. The probability that this grouping occurred by chance was modeled using an Excel VBA macro that randomly binned the images into four groups of four, 10,000 times (File S3). The final *p*-value was <0.0024 and deemed significant.

2.4. mRNA and mtDNA Quantitation

For quantitation of mRNA, fold change in each mRNA of interest was determined using the $\Delta\Delta C_t$ method normalized to the geometric mean of *cdc-42*, *pmp-3*, and *Y45F10D.4* [35]. For quantitation of mitochondrial DNA (mtDNA), PCR primer pairs targeting mtDNA-encoded *ctb-1* and intron 4 of genomic DNA-encoded *ama-1* were used as described [36].

The ratio of mitochondrial DNA to nuclear DNA was calculated using Real Time PCR, with *ama-1* serving as the nuclear normalization quantity [37]. A complete list of qPCR primers is provided in Table S5.

2.5. Mutation Screening Assays

Full methodological details of the *unc-93(e1500)* and *unc-58(e665)* reversion assays; the *eT1(III;V)* and *nT1(IV;V)* lethal mutation assays; the Lac-Z Frameshift Assay; and the 'terminal deoxynucleotidyl transferase dUTP nick end labeling' (TUNEL) assay are presented in File S1.

2.6. Nucleotide Extraction and Mass Spectrometry

The quantitation of deoxyribonucleotide and ribonucleotide species in whole-worm extracts of *isp-1(qm150)* and wild-type (N2) animals was undertaken using HPLC-MS at the UTHSCA Mass Spectrometry Facility. Methods for nucleotide extraction, separation, quantitation, and statistical analysis are provided in File S1.

2.7. R-Loop Quantification

R-loop formation in worms was quantified using α S9.6 primary antibody (Kerafast, 1:2000 in 5% Blotto, 16 h, 4 °C), previously shown to be selective for DNA::RNA hybrids [38]. A list of R-loop reagents, and detailed methodology describing their use, is provided in File S1.

2.8. Spliceosome Reporter Assays

egl-15 and *ret-1* alternate splicing reporter genes were engineered by Kuroyanagi and colleagues [39,40]. Details of reporter construction and their use are provided in File S1.

2.9. Nematode Oxygen Consumption

Nematode oxygen consumption measurements were undertaken using a Seahorse XFe24 Analyzer. Approximately 30 worms were added to each Seahorse well, with 5 replicate wells employed per test condition. We followed the procedure of Luz and colleagues [41], and only averaged oxygen consumption rates across the final four measurement phases for each well to provide a single rate value for that well. A total of four independent experiments were performed. Significance testing was undertaken using the Student's *t*-test, with $p < 0.05$ considered significant.

2.10. Polysome Profiling

Quantitative polysome profiling was undertaken using the procedure of Steffen and colleagues [42] using a Brandel BR-188 Density Gradient Fractionation System. Several modifications were included to optimize for *C. elegans* polysome extraction, and these are described in detail in File S1. Two fully independent, experimental replicates were collected.

2.11. Western Analysis

Western blotting reagents and suppliers are described in File S1.

2.12. DNA Damage Response (DDR) Screen

The *atm-1(gk186); atl-1(tm853)* suppressor screen was undertaken using a bacterial feeding RNAi targeting 201 DDR-related genes [43]. A protocol describing our screening method, including quantitation of the RNAi effect-size and significance testing, is provided in File S1 and Tables S1–S3.

3. Results

3.1. Loss of ATL-1/ATR Desensitizes Worms to Mitochondrial ETC Stress

In *C. elegans*, *atp-3* encodes the ortholog of the human ATP5O/OSCP subunit of the mitochondrial F₁F₀ ATP synthase, whereas *isp-1* encodes the Rieske Fe-S ortholog of

complex III. We have previously reported that wild type worms exposed to increasing amounts of bacterial feeding RNAi targeting either *atp-3* or *isp-1* reach a critical threshold, after which the concentration of RNAi causes worms to exhibit a reduction in body size and an extension of lifespan [44]. For *isp-1* RNAi, life extension follows a monotonic function, whereas for *atp-3* RNAi, life is first extended, and then it is pathologically shortened [44]. We previously mapped these functions using 12 point datasets across multiple rounds of testing [44]. The differing effect of *atp-3* and *isp-1* feeding RNAi on lifespan reflects the more potent degree of ETC inhibition that is ultimately attained following severe *atp-3* knockdown.

Using these well-defined treatment regimes, we tested whether loss of the checkpoint proteins ATM-1 and ATR altered the phenotypic response of worms to mitochondrial ETC disruption (see File S1 for a full description of mutants used in this study, and the method used to propagate lethal DDR mutations). When mutant *atm-1(gk186)* worms were exposed to *atp-3* or *isp-1* RNAi (1/10th strength and undiluted), animals matured and survived indistinguishably from similarly-treated wild type worms (Figure 1A–D). In contrast, *atl-1(tm853)* mutants were differentially refractory to the effects of knockdown of either RNAi. This effect was most evident in worms treated with 1/10th strength *atp-3* or *isp-1* RNAi, where animals showed obvious resistance to both size reduction (Figure 1A,B) and lifespan extension (Figure 1C,D) (additional examples are presented later in Figure 2A–C). *atp-3* and *isp-1* knockdown did eventually reduce adult size, and extend life in the mutant *atl-1(tm853)* background, suggesting the response to ETC disruption in these animals is right-shifted relative to wild type control (see schematic Figure 1C,D). Surprisingly, the measurement of *atp-3* and *isp-1* mRNA levels following RNAi treatment revealed that target gene knockdown was as efficacious in *atl-1(tm853)* mutants as it was in wild type worms (Figure 1E), indicating these animals were not deficient for RNAi. Furthermore, we found that *atl-1(tm853)* mutants were also refractory to mitochondrial ETC disruption induced using chemical inhibition (Figure S1). Based on these findings, we conclude that inhibition of the phosphoinositide 3-kinase-related kinase ATL-1 confers resistance to mitochondrial ETC disruption.

3.2. MAK-1 and MAK-2 Participate in Mitochondrial Retrograde Response Signaling

During the course of our studies, we made the unexpected observation that two independently-generated *atm-1(gk186); atl-1(tm853)* double mutants regained sensitivity to *atp-3* and *isp-1* knockdown (Figure 1). This observation provides additional support for the notion that the RNAi machinery is unaffected by the loss of *atl-1*. To explain this odd finding, we reasoned that ETC disruption might normally induce DNA damage that activates ATR, but not ATM. In the absence of both ATR and ATM, however, secondary forms of DNA damage might accumulate that specifically trigger a third checkpoint response that reinstates sensitivity to *atp-3* and *isp-1* knockdown. This hypothesis reflects the well-established redundancy in the DNA damage response network [20]. Several recent studies by us and others [13,36,37] have shown a role for MAPK signaling following ETC disruption in worms. Interestingly, the p38 MAPK-activated protein kinases MAPKAP-2 and MAPKAP-3 are checkpoint proteins known in humans to act in parallel to ATM and ATR [45–47]. To explore the possibility that alternate checkpoint signaling is activated in PIKK mutant worms following ETC disruption, we exposed animals to *atp-3* knockdown, and simultaneously inhibited production of either MAK-1 or MAK-2, the worm orthologs of MAPKAP-2 and -3, respectively. The effect of these treatments on *atl-1(tm853)* and *atm-1(gk186)* single mutants, *atm-1(gk186); atl-1(tm853)* double mutants, and wild type worms was examined. Our results can be summarized as follows: (i) knockdown of *mak-1* or *mak-2*, either alone or in combination with *atp-3* knockdown, had no effect on final adult size in any of the genetic backgrounds (Figure 2A). (ii) Knockdown of *mak-1* or *mak-2* failed to reproducibly prevent life extension following *atp-3* inhibition in the two independent *atm-1(gk186); atl-1(tm853)* double mutant isolates. (iii) Unexpectedly, the reduced ability of *atp-3* RNAi to extend the lifespan of *atl-1(tm853)* mutants was further impaired when

undertaken in conjunction with *mak-1* or *mak-2*. A similar result was also observed for the *atm-1(gk186)* mutant. (iv) For wild type worms, only *mak-1* knockdown significantly impaired *atp-3* RNAi-induced life extension (Figure 2B,C). These findings suggest that at least two other checkpoint proteins, namely MAK-1 and MAK-2, are causally involved in lifespan extension (but not size determination) of worms experiencing mitochondrial ETC disruption. The role of different checkpoint proteins is, therefore, dependent upon the functional status of both ATL-1 and ATM-1. When these two checkpoint proteins are disrupted simultaneously, MAK-1 and MAK-2 become dispensable, potentially implying yet another checkpoint system awaits identification in *atm-1(gk186); atl-1(tm853)* double mutants. Although clearly complicated, this is not unexpected for a response that is network-based and sensitive to a variety of DNA lesions.

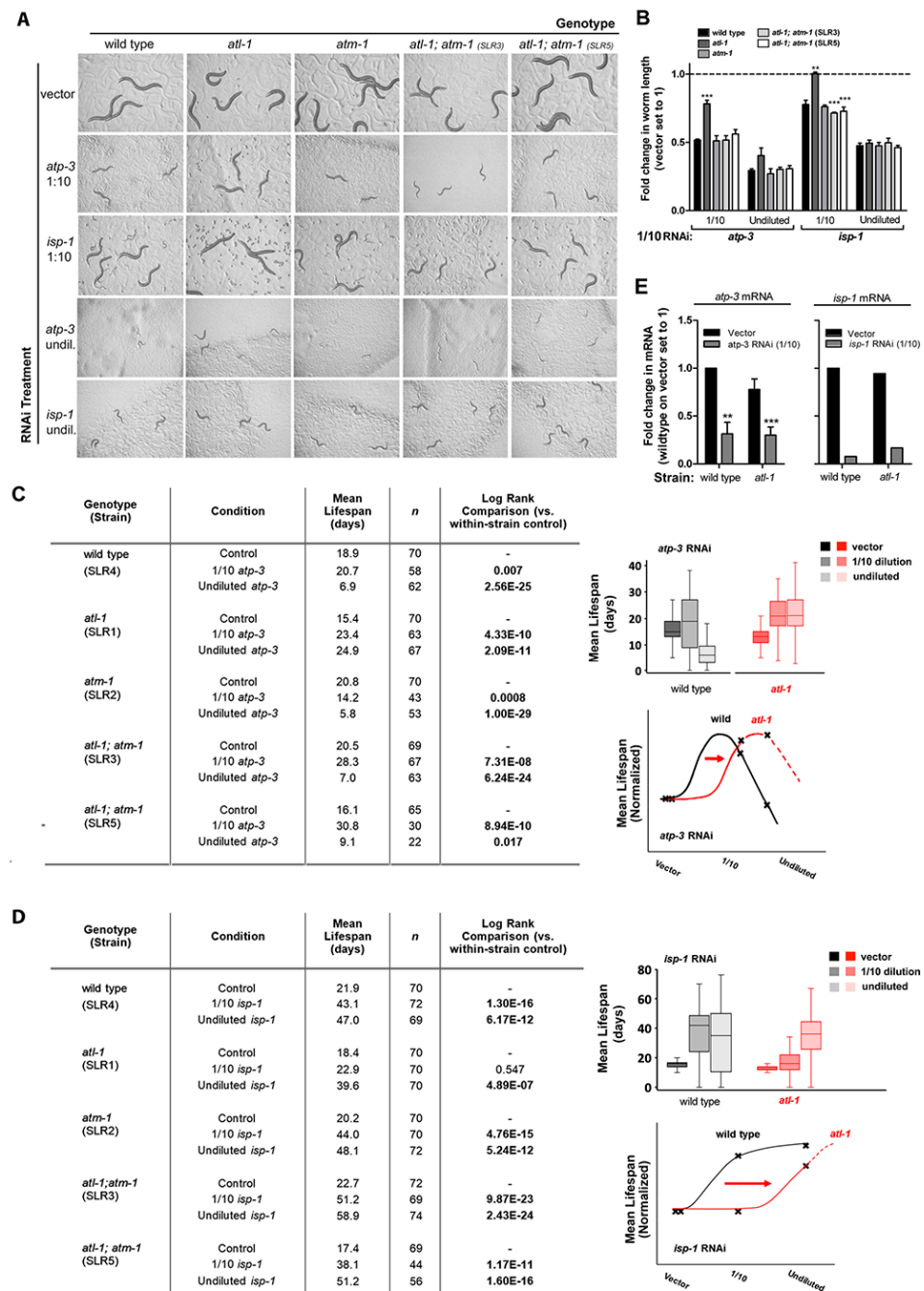


Figure 1. Loss of ATL-1 desensitizes worms to mitochondrial respiratory chain stress. (A,B) *atl-1(tm853)*

knockout mutants are resistant to size reduction induced by *atp-3* or *isp-1* bacterial feeding RNAi (panel A). Tested worms include wild type, *atm-1(gk186)* and *atl-1(tm853)* single mutants, as well as two independent *atl-1(tm853); atm-1(gk186)* lines. Worm length is quantified in panel B. All worms were seeded at the same time. Each row was photographed at a common time interval after seeding. This interval increased with increasing RNAi potency, since worms matured more slowly. Evident across rows are differences in growth rates when strains are cultured on the same RNAi treatment. In (B), error bars refer to SEM. Asterisks refer to significant difference relative to respective wild type sample (Students' *t*-test): ** $p < 0.01$, *** $p < 0.001$. (C,D) Charts on left: Adult lifespan of worm strains tested in (A). Shown is a representative study. Samples listed in each table were tested in parallel. For each strain, a synchronous population of 8000 eggs was distributed over the three relevant test conditions. After hatching, unbalanced worms were retrieved (~1/16th). Replicate data for *atp-3* are presented in Figure 2. Right panels: (Top) Box plots showing lifespan distribution of selected worm populations from chart on left. Box shows mean \pm 25%. Bars: 5–95%. (Bottom) Schematics illustrating the right-shifting effect of *atl-1* removal on mean lifespan following exposure to *atp-3* and *isp-1* feeding RNAi. Curve shapes are based on the 12-point RNAi data collected in Rea et al. [44]. (E) RNAi knockdown efficacy is not altered in *atl-1(tm853)* mutants. mRNA levels were quantified by q-RT PCR following exposure to 1/10th strength *atp-3* or *isp-1* bacterial feeding RNAi ($n = 3$ and $n = 1$ experimental replicates, respectively). Error bars: SEM. Significance testing: Student's *t*-test. Asterisks refer to difference relative to wild type vector control: ** $p < 0.01$, *** $p < 0.001$. In (A–E), the wild type control line (SLR4) was deliberately moved into the nT1 genetic background as the appropriate control (see Section 2).

3.3. Knockdown of DNA Pol α Reverses the Small Phenotype of *atm-1(gk186); atl-1(tm853)* Mutants

To further explore the role of novel checkpoint proteins in modulating the critical ETC threshold in *atm-1(gk186); atl-1(tm853)* double mutants, we undertook a double RNAi screen of 201 DNA damage response-related genes. We asked whether knockdown of a target gene in this genetic background could re-confer resistance to *atp-3* knockdown, similar to *atl-1(tm853)* mutants (for screen details, see Figure 3A). We identified two genes: *scc-3*, which encodes a cohesin complex subunit; and Y47D3A.29, which is orthologous to the human PolA1 catalytic subunit of DNA polymerase alpha (DNA pol α , Figure 3B,C). The effect of losing each gene was robust to three different post-hoc tests (each $p < 0.001$, see Tables S1–S3, File S2, and Methods for details of statistical testing). The isolation of PolA1 is particularly intriguing because it suggests that *atp-3* knockdown in *atm-1(gk186); atl-1(tm853)* double mutants could be inducing some kind of disruption to DNA, its repair, or its replication, and which is bypassable by low-fidelity polymerases (which presumably accommodate knockdown of PolA1). This, in turn, might avoid checkpoint activation and make animals appear more *atl-1(tm853)*-like in our assay.

3.4. No Evidence for Permanent Nuclear DNA Damage Following Mitochondrial ETC Disruption

Nuclear DNA (nDNA) damage is the canonical signal that results in activation of ATR. In worms, resected ends of dsDNA breaks, and stalled replication forks have both been shown to activate ATL-1 [48]. Both lesions contain single-stranded DNA (ssDNA), and binding of heterotrimeric replication protein A (RPA) to these regions, in turn, recruits and activates ATL-1. To test if ETC disruption results in elevated levels of dsDNA breaks, we focused on *isp-1(qm150)* genetic mutants, since no viable *atp-3* mutant exists, and utilized TUNEL staining on sections of paraffin-embedded worms [49]. We found no evidence for increased nDNA breakage (Figure S2A). DNA repair is sometimes inaccurate, depending on the repair machinery that is employed. To test if DNA mutation frequency was increased in worms exposed to ETC disruption, we employed four independent genetic assays. To facilitate analysis, these studies were undertaken using *atp-3* RNAi. The *eT1(III;V)* and *nT1(IV;V)* reciprocal chromosomal translocations each suppress recombination against the regions they balance (~15 Mbp for both balancers). Homozygous-lethal DNA mutations, therefore, accumulate on balanced chromosomes, and they become identifiable when the

balancing eT1 chromosomal pair, or the nT1 chromosomal pair, are lost because unbalanced progeny that are homozygous for the mutation are inviable and, hence, absent. Using both assays, we found no evidence for increased nDNA mutation rate following knockdown of *atp-3* in wild type worms (Figure 4A). Similarly, the use of two Unc phenotypic reversion assays yielded similar conclusions (Figure 4B). Taken together, our data show there is neither an increase in DNA strand breakage nor is there an increase in nuclear DNA mutation frequency in worms experiencing mitochondrial ETC dysfunction.

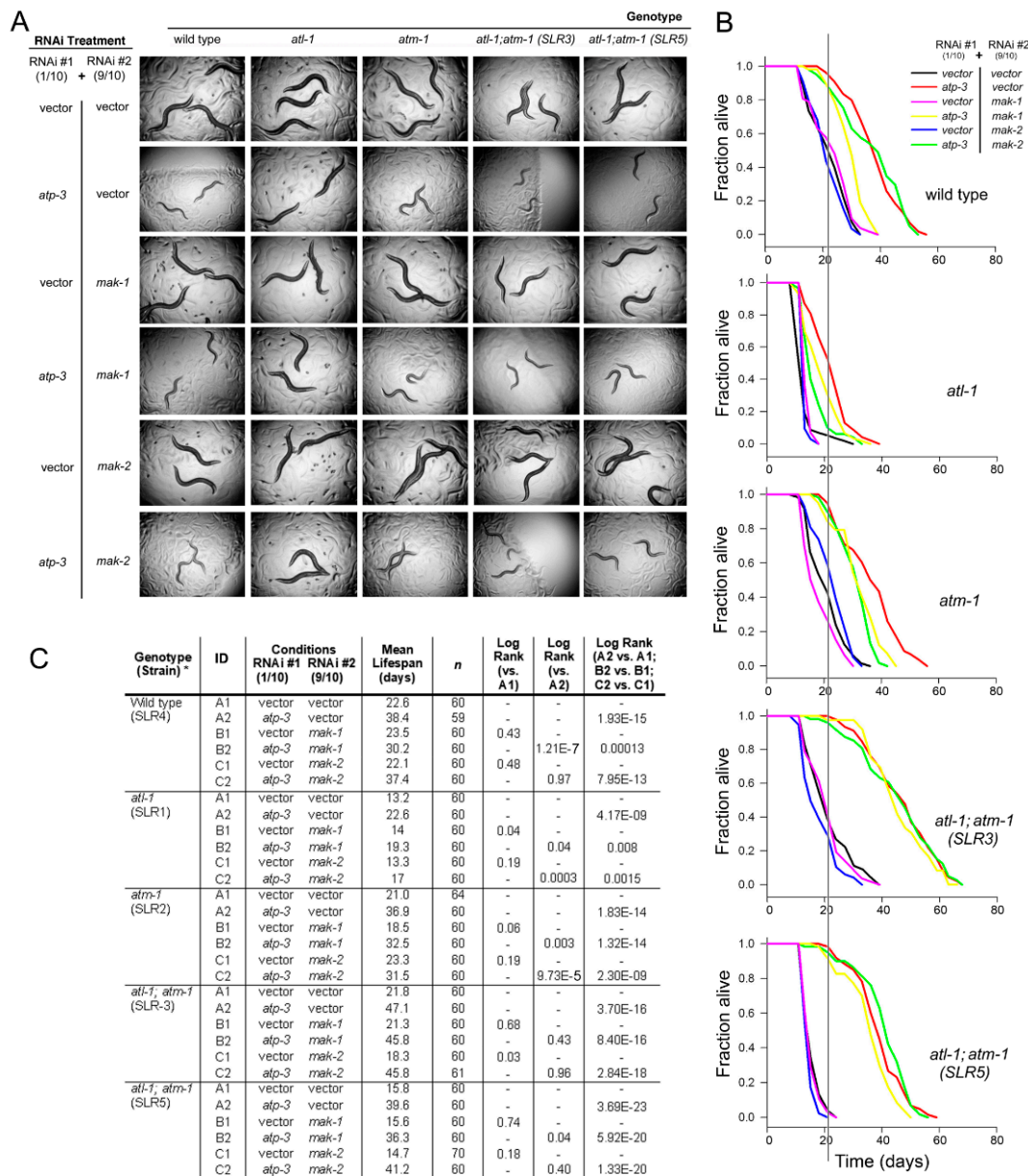


Figure 2. MAPKAP kinases are active following mitochondrial respiratory chain stress. (A–C) The MAPKAP kinases MAK-1 and MAK-2 play no role in size control of worms exposed to 1/10th strength *atp-3* feeding RNAi (A); however, they do control lifespan in wild type worms and in *atm-1* (*gk186*) and *atf-1* (*tm853*) single gene mutants (B,C). Worms in (A,B) were established independently using a total of 8000 and 32,000 synchronized eggs, respectively, and all conditions in each panel were tested in parallel. In (A), worms were photographed at the same chronological point. In (B), the vertical line marks median survival of wild type worms on vector control RNAi. In (A–C), all worms are the unbalanced F1 progeny of parents carrying the *nT1* reciprocal chromosomal translocation. * Full genotypic information provided in Table S4.

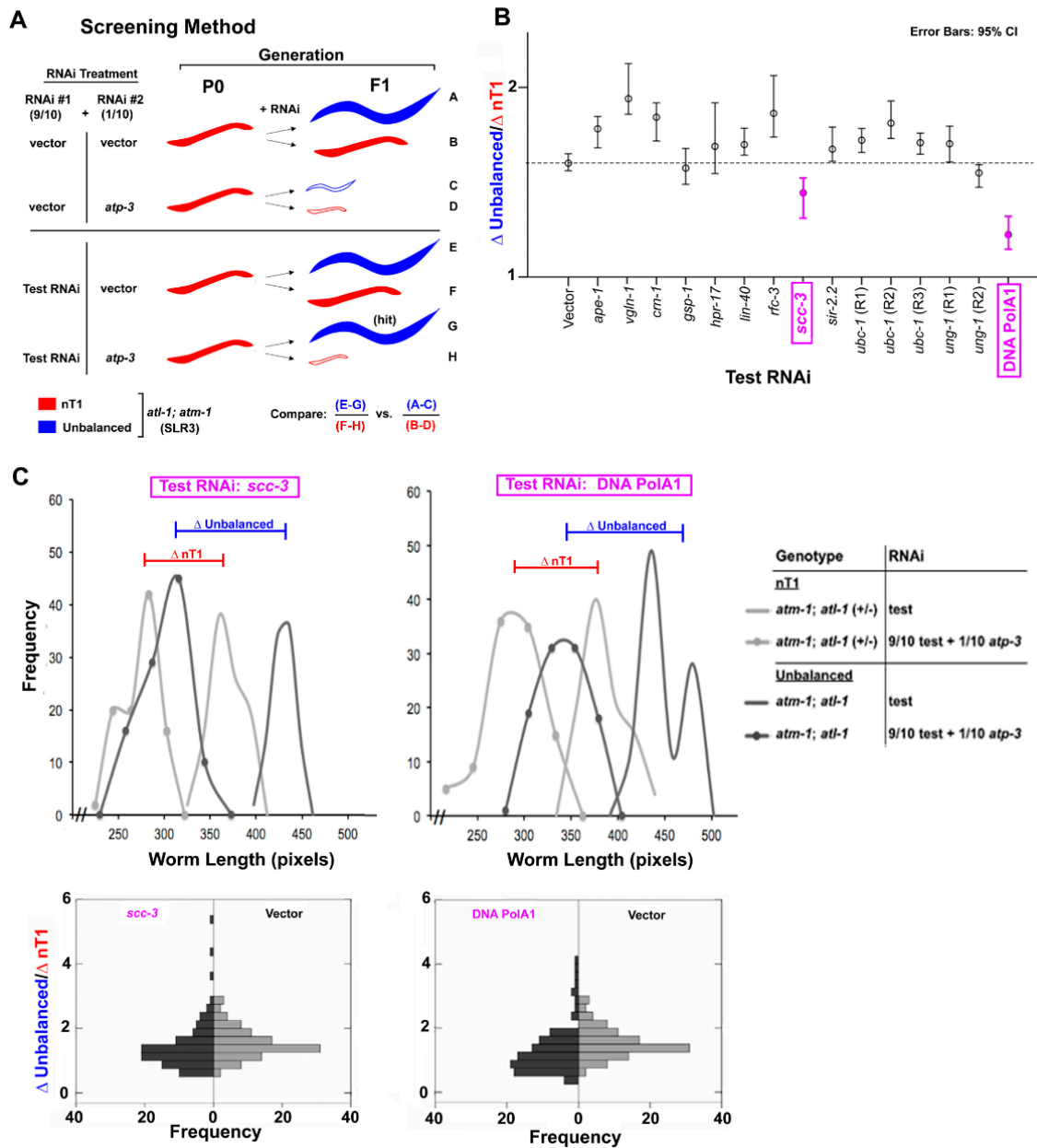
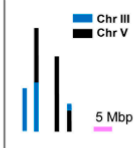
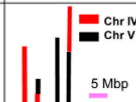
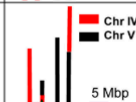


Figure 3. Screen for additional checkpoint proteins activated by mitochondrial ETC dysfunction. (A) Schematic of RNAi screen used to identify DNA damage response genes active in *atl-1(tm853); atm-1(gk186)* double mutants following *atp-3* knockdown. Test RNAi that differentially counteracted the size-reducing effect of 1/10th strength *atp-3* RNAi in unbalanced *atl-1(tm853); atm-1(gk186)* worms, but not nT1-containing *atl-1(tm853); atm-1(gk186)/+* worms, were sought (hit). (B) Results of RNAi screen. The effect of each test RNAi on the length of unbalanced worms and nT1-containing worms in the presence and absence of 1/10th strength *atp-3* RNAi is reported as a mean difference ratio. The 95% confidence interval (CI) for each ratio is shown. RNAi knockdown of *scc-3* and *Y47D3A.29* (labeled DNA PolA1) both significantly reduced the mean ratio relative to vector-only test RNAi ($p < 0.001$, see Methods for significance testing procedure). (C) *Top row:* Size distribution of worm populations treated with *scc-3* (left) or *Y47D3A.29* (right) feeding RNAi. *Bottom row:* Histograms of mean difference ratios for worm populations treated with *scc-3* (left) or *Y47D3A.29* (right) feeding RNAi, and plotted relative to worms treated with vector in place of test RNAi. Mean difference ratios were generated by random sampling from the distributions in the *top row*.

A

Genotype	Genome Coverage *	<i>atp-3</i> : Vector RNAi Ratio	F1 Animals Scored	Mutants Detected	Mutant Frequency (%)	Fisher's Exact Test P-value
<i>dpy-18(e364)/eT1 III</i> ; <i>unc-46(e177)/eT1 V</i> .		Vector	152	0	0	--
		1:200	173	0	0	1
		1:100	187	0	0	1
		1:50	187	0	0	1
		1:20	177	0	0	1
1:10	187	1	0.5	1		
nT1 (IV;V)		Vector	1292	4	0.31	--
		1:20	858	5	0.58	0.497
nT1 (IV;V) (<i>qls50</i>)		Vector	671	1	0.15	--
		1:20	674	0	0.00	0.499

*Chromosomes drawn to scale. Green star in schematic indicates the presence of GFP marker.

B

Genotype	RNAi (Dilution)	Plates Scored	Plate Reversion Frequency (%)	Fisher's Exact Test P-value
<i>unc-58</i> (<i>e665</i>)	Vector	63	0	--
	<i>atp-3</i> (1:20)	63	0	1
	<i>rpa-1</i> (1:10)	64	23.4	<0.001
<i>unc-93</i> (<i>e1500</i>)	Vector	48	27.1	--
	<i>atp-3</i> (1:20)	88	22.7	0.687
	<i>rpa-1</i> (1:10)	36	63.9	0.001

Figure 4. Nuclear DNA mutation rate is not increased following mitochondrial ETC disruption. (A,B) Multiple genetic screens reveal no significant increase in nuclear DNA mutation frequency following knockdown of *atp-3* ($p > 0.05$, Fisher's exact test). Phenotypes scored include lethal nuclear DNA mutation events covered by the eT1 and nT1 chromosomal translocations (A), and recovery of wild type movement in *unc-58(3665)* and *unc-93(e1500)* mutants (B). Knockdown of replication protein A (*rpa-1*) was included as a positive control in (B).

3.5. Ribonucleotide and Deoxyribonucleotide Pools Are Disrupted by Mitochondrial ETC Dysfunction

To search for alternate mechanisms by which ATL-1 might be activated in worms experiencing mitochondrial ETC dysfunction, we examined changes in whole-worm nucleotide levels. As in humans, pyrimidine biosynthesis in *C. elegans* requires a functional mitochondrial electron transport chain. This is because formation of orotate from dihydroorotate is coupled to reduction of ubiquinone (UQ) in a reaction catalyzed by the inner mitochondrial membrane enzyme, dihydroorotate dehydrogenase (DHODH, Figure S3). In mammals, processes that slow flux through the mitochondrial ETC, downstream of UQ, also slow the rate of dihydroorotate dehydrogenase, resulting in measurable disruption of nucleotide pools [50]. Several important enzymes are sensitive to changes in nucleotide abundance, including DNA polymerases which are rate-limited by availability of their deoxyribonucleotide substrates [51]. Stalling of DNA polymerase, followed by continued DNA unwinding by the MCM helicase, results in ssDNA formation [52,53], which is a known substrate for ATR activation.

To measure nucleotide levels, we re-focused our attention on the *isp-1(qm150)* genetic mutant for ease of culture. We interrogated three stages of development—the final two stages of larval development (L3 and L4), and the first day of adulthood. These stages were selected because in wild type worms, there is a heavy demand for nucleotide precursors around the L3/L4 molt, and then again around the L4/adult molt. At these times, the gonad arms are expanding, and there is also a concomitant five-fold and a six-fold increase in mitochondrial DNA (mtDNA), respectively [54]. Among nine deoxyribonucleotide

species that we were able to resolve and reliably detect (see Methods), we observed significant increases in dCDP and dTMP in L4 larvae of *isp-1(qm150)* mutants (Figure 5A). The increase in dCDP abundance was maintained into adulthood (Figure 5B). Among eleven ribonucleotide species that we were able to reliably resolve and detect, we observed significant increases in AMP, CMP, and UMP in L4 larvae of *isp-1(qm150)* mutants (Figure 5C). This was accompanied by a significant decrease in the level of GTP. In adult *isp-1(qm150)* worms, changes in ribonucleotide pools became more pronounced, with eight species being significantly underrepresented—ADP, ATP, GDP, GTP, CMP, CTP, UDP, and UTP (Figure 5D). Changes in nucleotide pools were specific to L4 and adult worms, since we did not detect any measurable differences in any quantifiable nucleotide species in L3 larvae of *isp-1(qm150)* mutants relative to wild type worms (Figure 5E). Finally, the absence of a corresponding increase in many of the monophosphate ribonucleotide species in adult *isp-1(qm150)* worms when their corresponding di- and triphosphate counterparts decreased suggests ribonucleotide pool sizes are reduced in these animals. We combined the levels of each mono-, di-, and triphosphate species, and tested if they differed significantly between strains at each developmental stage, but they did not. Error propagation, however, severely reduced our statistical resolving power (Figure 5F). Collectively, we conclude that disruption of the mitochondrial ETC in *C. elegans* results in measurable and significant changes in the abundance of multiple nucleotide species, notably with all ribonucleotide triphosphate species becoming underrepresented by adulthood.

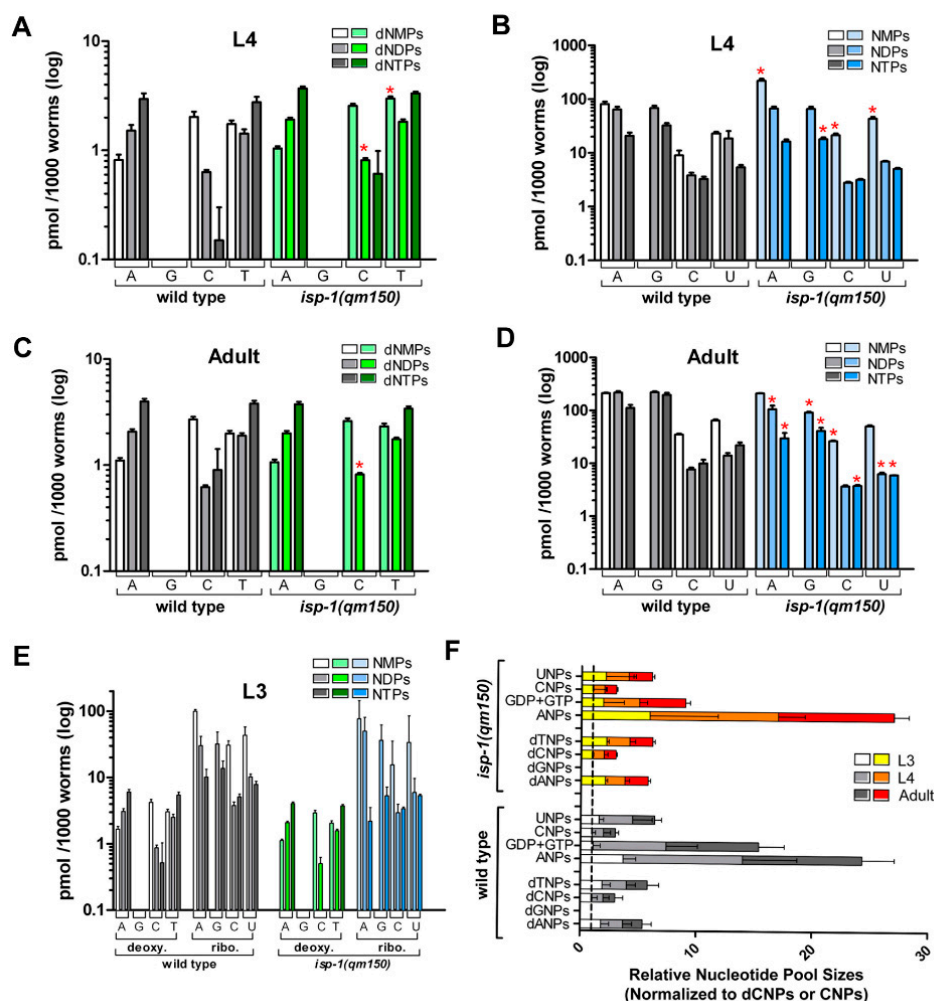


Figure 5. Ribonucleotide and deoxyribonucleotide pool ratios are disrupted following mitochondrial ETC disruption. (A–E) Absolute levels of deoxyribonucleotide (A,C) and ribonucleotide (B,D) species in wild type (N2) and *isp-1(qm150)* worms at the L4 and day-one adult stages, measured using quantitative

LC-MS. Red asterisks indicate nucleotide quantities that differ significantly between strains (Student's *t*-test, 5% FDR). Four nucleotides were not measurable by our assay (dGMP, dGDP, dGTP, GMP). No significant differences in any nucleotide level existed between strains at the L3 larval stage (E). (F) Relative nucleotide pool sizes in L3, L4 and day-one adult N2 and *isp-1(qm150)* worms, determined by summing together the mono-, di-, and triphosphate species of each deoxyribonucleotide or ribonucleotide (guanosine was an exception) and normalizing to dCNP or CNP, respectively, across each larval stage. No significance difference in each respective nucleotide pool size between strains was detected (Student's *t*-test, 5% FDR; $n = 3, 7$ and 3 experimental replicates for N2 L3, L4, and adult worms; and $n = 3, 5$, and 3 for *isp-1(qm150)* L3, L4, and adult worms, respectively).

3.6. Evidence for RNA Polymerase Stalling Following Mitochondrial ETC Disruption

Stalling of RNA polymerase II (RNA pol II) during transcription is sufficient to activate an ATR, RPA, and p53-dependent DNA damage response in human fibroblasts [55]. Given that mitochondrial ETC dysfunction in *isp-1(qm150)* mutants leads to measurable reductions in all four ribonucleotide triphosphates, and because we have previously shown a role for p53/*cep-1* in the life extension of these worms [17], we hypothesized that ATL-1 activation following ETC disruption might occur as a result of RNA pol II stalling due to reduced nucleotide availability. We therefore quantified the formation of R-loops on genomic DNA [56]. R-loops are DNA:RNA hybrids that accumulate when transcription stalls (Figure 6A). We detected R-loops in purified, whole-worm genomic DNA fractions using slot blot analysis in conjunction with a DNA:RNA hybrid-specific antibody (α S9.6) [38]. To obtain sufficient material for these studies, we utilized a double feeding RNAi approach, and tested four conditions: wild type worms exposed to either vector control RNAi, 1/10th strength *isp-1* RNAi, 9/10th strength *atl-1* RNAi, or both 9/10th strength *atl-1* RNAi with 1/10th strength *isp-1* RNAi. Vector control feeding RNAi was added as balancer where appropriate. qRT-PCR analysis undertaken before the start of the experiment revealed 9/10th strength *atl-1* RNAi reduced *atl-1* mRNA by 50% (Figure 6B), the same amount that was observed in maternal-effect rescued *atl-1(tm853)* mutants (Figure 6C). The results of our R-loop studies can be summarized as follows (Figure 6D): (i) knockdown of *isp-1* significantly enhanced R-loop formation relative to vector control (Student's *t*-test, $p < 0.05$). (ii) Knockdown of *atl-1* did not block R-loop formation by *isp-1*, as would be expected for a gene that functioned downstream of R-loop accumulation. We next tested whether any differences in DNA:RNA polymer length distinguished R-loops generated in worms exposed to *isp-1* RNAi from those exposed to *isp-1* and *atl-1* double RNAi. Genomic fractions were separated on an agarose gel, stained with ethidium bromide, then transferred to nitrocellulose and probed with α S9.6 antibody (Figure 6E). No overt difference distinguished the two samples; however, in both instances, we noted some of the staining with α S9.6 localized to low molecular weight DNA:RNA fragments (<2 kb), in addition to the higher molecular weight structures that we expected. The identity of these smaller fragments remains uncharacterized (see Section 4). Collectively, our studies suggest that transcriptional stalling is increased in worms exposed to mitochondrial ETC disruption, identifying one route by which ATL-1 is potentially activated in these animals.

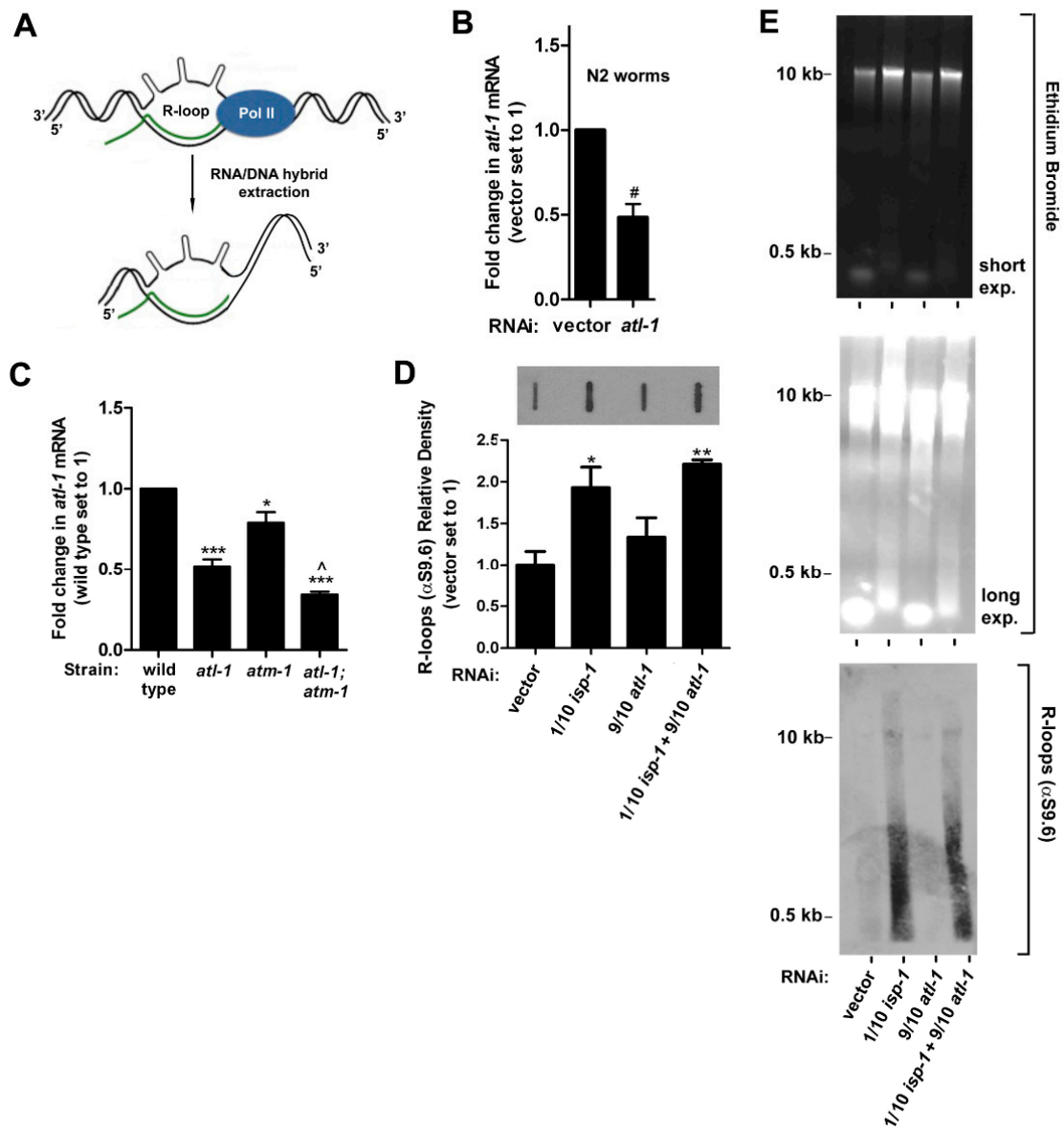


Figure 6. Evidence for RNA Pol II stalling following mitochondrial ETC stress. (A) Schematic showing genesis of R-loops following stalling of RNA Polymerase II. Modified from [57]. (B,C) RNAi knockdown of *atl-1* in wild type (N2) worms reduces *atl-1* transcript abundance to the same extent as in maternal-effect *atl-1(tm853)* mutants. In (C), all worms are unbalanced F1 progeny from parents carrying the nT1 reciprocal chromosomal translocation ($n = 3$; error bars: SEM; significance testing: Student's *t*-test; symbols: significantly different from wild type: * $p < 0.05$; *** $p < 0.001$; significantly different from *atl-1(tm853)*: ^ $p < 0.05$). In (B), $n = 2$ and # marks range. (D) R-loops are significantly increased in N2 worms following knockdown of *isp-1* (1/10th RNAi strength). Combined knockdown of *isp-1* (1/10th RNAi strength) and *atl-1* (9/10th RNAi strength) does not abrogate R-loop accumulation. Top panel: representative immunoblot of R-loops; bottom panel: immunoblot quantitation: $n = 3$; error bars: SEM; Student's *t*-test (vs. vector): * $p \leq 0.05$, ** $p \leq 0.01$. (E) Samples in (D) were further analyzed by agarose gel electrophoresis (top two panels), and then western blotting using an antibody that cross reacts with DNA::RNA hybrids (α S9.6, bottom panel). Knockdown of *isp-1* results in an increase of gDNA-associated R-loops and unknown small molecular weight DNA::RNA hybrids.

3.7. RNA Splicing Is Not Altered by Mitochondrial ETC Disruption

Having identified a possible mechanism by which ATL-1 is activated in worms experiencing mitochondrial ETC stress, we next sought to determine the mode by which ATL-1 acts to further disrupt mitochondrial function. It is well-established that pre-mRNA splicing is a co-transcriptional process [58], and it has also been reported that *isp-1(qm150)* mutants are sensitive to knockdown of two spliceosome factors, SFA-1 and REPO-1, fully ablating their life extension [59]. We therefore tested whether the stalling of RNA pol II altered either splicing efficiency or splicing fidelity in worms exposed to ETC disruption, and if ATL-1 played a role in this process. We used two synthetic-gene reporter assays developed by Kuroyanagi and colleagues [39,60], designed to measure alternate splicing at the *egl-15* and *ret-1* loci, respectively. The latter reporter was shown to be a sensitive marker of age-related splicing dysfunction [59]. Each assay has the potential to produce two fluorescent outputs that record changes in the nature of a differential splicing event, and the tissues in which these events occur (Figure S4A,B). We exposed worms carrying the relevant reporter cassette to double feeding RNAi targeting *atp-3* or *isp-1* (1/10th strength) in conjunction with either *atl-1* or vector control (9/10th RNAi strength) (Figure S4C). Animals were followed three days into adulthood. None of the conditions that disrupted the mitochondrial ETC, neither in the presence or absence of *atl-1*, resulted in alteration of *egl-15* or *ret-1* splicing relative to vector control-treated animals.

3.8. Reduced ATL-1 Activity Does Not Enhance Hormetic Stress Response Activation

We next tested whether the loss of *atl-1* affected the activity of major stress response pathways known to be activated by *atp-3* or *isp-1* depletion [3,13,44,61]. The loss of *atl-1* did not result in constitutive activation of *Phsp-6::GFP*, *Pgst-4::GFP*, or *Ptbb-6::GFP*, which are markers of ATFS-1, SKN-1/NRF-2, and PMK-3/p38 activation, respectively (Figure S5A–D); and neither did the loss of *atl-1* increase gene expression of *sod-3*, *ugt-61*, or *hsp-6* (Figure S5E). These results indicate that the reduction of *atl-1* does not affect typical mitochondrial stress response pathways.

3.9. Oxygen Consumption Remains Surprisingly Unaltered in *atl-1* Mutants Exposed to ETC Disruption

We next tested whether mitochondria in *atl-1(tm853)* mutants were inherently different from those of wild type worms. We also analyzed mitochondria from *atm-1(gk186)* single mutant worms, as well as *atl-1(tm853); atm-1(gk186)* double mutants. Properties that we examined included mitochondrial DNA (mtDNA) content, nuclear-encoded ETC transcript abundance, mitochondrial morphology, and whole-worm oxygen consumption. Our findings can be summarized as follows: relative to wild type worms, mtDNA copy number is halved in *atl-1(tm853)* mutants, consistent with an earlier report [62]. mtDNA content was also halved in *atl-1(tm853); atm-1(gk186)* double mutants (Figure 7A). To assess changes in nuclear-encoded ETC transcript abundance, we focused on five genes: *nuo-6*, *mev-1*, *isp-1*, *cco-1*, and *atp-3*, representing subunits from mitochondrial complexes I through V, respectively. We found that all transcripts except *nuo-6* were significantly decreased relative to wild type worms in all three mutant strains studied. The only exception was *mev-1*, for which mRNA levels remained unchanged in *atm-1(gk186)* mutants (Figure 7B).

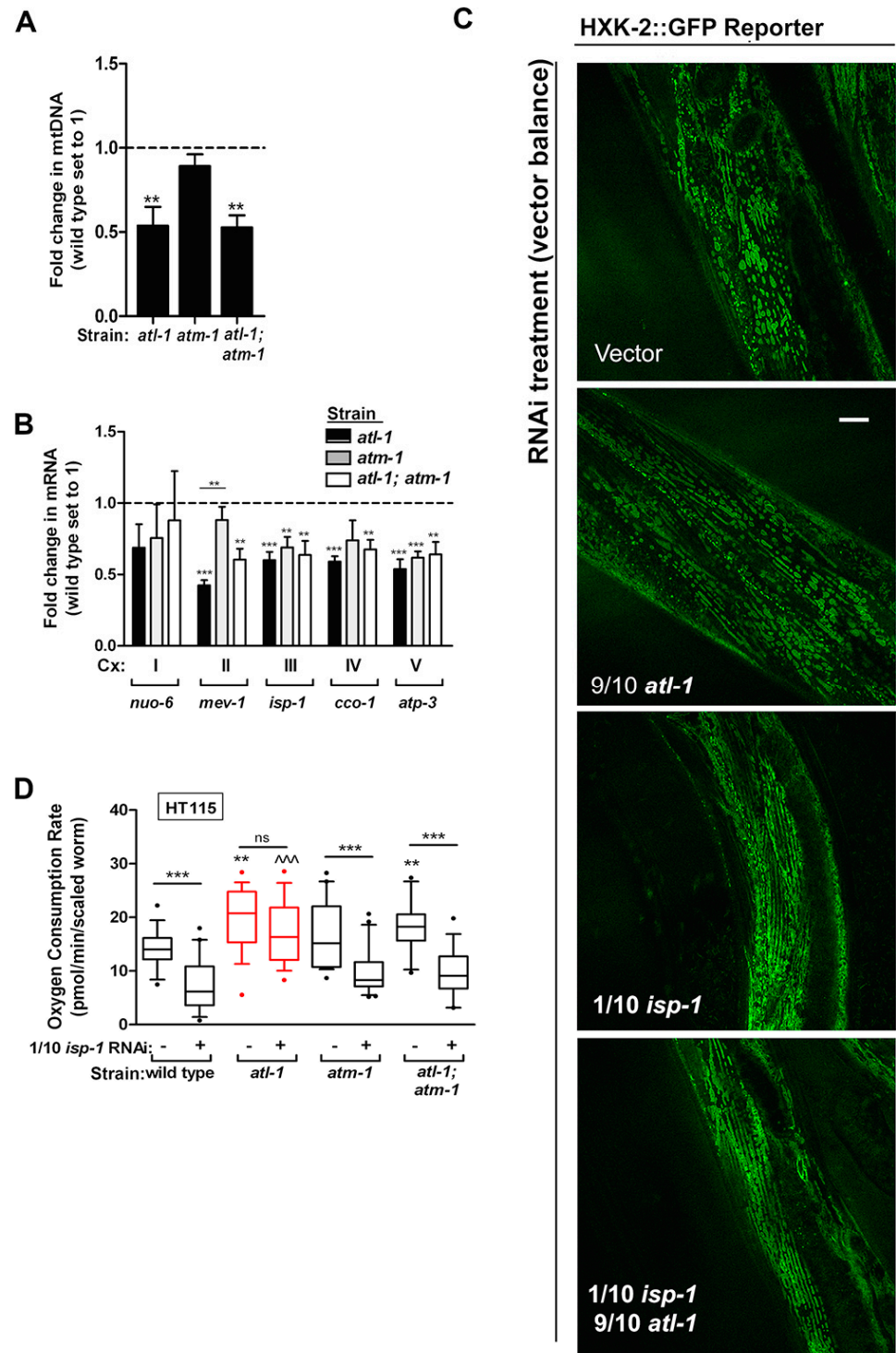


Figure 7. *atl-1(tm853)* mutants maintain normal oxygen consumption when confronted with disruption of their mitochondrial ETC. (A) Mitochondrial DNA abundance is significantly decreased in *atl-1(tm853)* mutants compared to wild type worms ($n = 3$). (B) Transcript abundance of nuclear-encoded ETC genes is significantly decreased in *atl-1(tm853)* mutants relative to wild type worms ($n = 3$; Cx: complex). (C) Morphology of body-wall muscle mitochondria assessed using HXK-2::GFP [63], following *atl-1* knockdown in the absence or presence of mitochondrial ETC disruption (1/10th strength *isp-1* RNAi). Both *atl-1* and *isp-1* knockdown significantly alter mitochondrial morphology relative to vector-control ($p < 0.0024$, refer to Methods for significance testing). Scale bar:

20 microns. (D) *atl-1(tm853)* mutants are resistant to changes in oxygen consumption following *isp-1* knockdown (1/10th strength RNAi). All other tested strains experienced a significant decrease in oxygen consumption ($N = 4$). Oxygen consumption was measured using a Seahorse XFe24 Analyzer. In (A,D), all worms are the unbalanced F1 progeny of parents carrying the nT1 reciprocal chromosomal translocation. In (A–D), asterisks indicate a significant difference from wild type (Student's *t*-test) unless otherwise noted by a bar for the relevant comparison group: ** $p < 0.01$. *** $p < 0.001$; ns, not significant. In (D), ^^^ $p < 0.001$ in comparison to wild type on *isp-1* RNAi. In (A,B), error bars are SEM; in (D), box and whisker plots show 10–90 percentile, with outliers marked (dots).

To quantify changes in mitochondrial morphology, we employed a hexokinase-2::GFP translational reporter (HXK2::GFP) that is localized to the outer mitochondrial membrane [63]. We observed a significant increase in the number of fused mitochondria in reporter worms treated with *isp-1* RNAi ($p < 0.0024$, see Methods for details of statistical testing). Co-knockdown of *atl-1* did not significantly affect this result. Mitochondria in worms treated only with *atl-1* RNAi were indistinguishable from those of wild type animals (Figure 7C). Finally, the most significant finding that we uncovered was related to alterations in oxygen consumption by *atl-1(tm853)* mutants. When wild type worms, *atl-1(tm853)* and *atm-1(gk186)* single mutants, as well as *atl-1(tm853); atm-1(gk186)* double mutants were cultured on *isp-1* RNAi, the basal oxygen consumption rate of *atl-1(tm853)* mutants, as well as *atl-1(tm853); atm-1(gk186)* double mutants, significantly increased relative to wild type worms (Figure 7D). Moreover, though *isp-1* knockdown uniformly decreased oxygen consumption in wild type worms, *atm-1(gk186)* single mutants and *atl-1(tm853); atm-1(gk186)* double mutants, and by the same extent, oxygen consumption in *atl-1(tm853)* surprisingly remained unchanged following this treatment. We conclude that though *atl-1(tm853)* mutants contain half as much mtDNA as wild type worms and have a reduced abundance of several nuclear-encoded ETC transcripts, these worms surprisingly maintain normal oxygen consumption, even when confronted with disruption of their mitochondrial electron transport chain.

3.10. Loss of ATR Leads to Recovery of Translational Activity in Worms Exposed to ETC Disruption

Several mechanisms could explain how *atl-1(tm853)* mutants maintain oxygen consumption despite ETC disruption. Any process that ultimately increases flux or efficiency of the respiratory chain could be involved. Enhanced supercomplex formation, elevated matrix Ca^{2+} , modification of ETC subunits, or simply enhanced translational output of respiratory subunits could all be behind the unique respiratory response seen in *atl-1(tm853)* mutants. We focused on translational output because there is evidence from human 293T cells that ATR might directly regulate the ribosomal machinery by affecting phosphorylation of the nascent polypeptide-associated complex (NAC) [20]. In worms, ICD-1 is the sole β NAC isoform [64,65]. Although the ATR phosphorylation site of human BTF3/ β NAC is not conserved in ICD-1, we observed, by western analysis, that ICD-1 protein levels are selectively elevated in *atl-1(tm853)* mutants following *atp-3* knockdown (*isp-1* knockdown was not tested due to limited quantities of antisera, see Section 2) (Figure 8A). Moreover, early analyses involving several hundred microarray datasets [66] showed *icd-1* formed part of a tightly clustered gene co-expression group (Figure 8B) that is significantly enriched (hypergeometric distribution, $p < 0.05$) for genes encoding ribosomal and mitochondrial ETC subunits, as well as key translational regulatory factors (Figure 8C). We therefore tested whether global translational activity was downregulated by mitochondrial ETC disruption, and if the loss of *atl-1* permitted its recovery. We employed polysome profiling in conjunction with RNAi targeting both *isp-1* (1/10th RNAi strength) and either *atl-1* or vector (both at 9/10th RNAi strength). We found that the actively translating polysome fraction of worms treated with *isp-1* RNAi was decreased by half relative to vector control-treated worms. Strikingly, simultaneous removal of both *atl-1* and *isp-1* restored polysome activity to wild type levels (Figure 8D). Loss of *atl-1* in the absence of ETC disruption did not significantly impact polysome abundance relative to wild type worms. These

data imply that ATL-1, when activated by mitochondrial ETC disruption, normally acts to dampen global ribosomal translation. Whether this is through a novel phosphorylation site on ICD-1, the downregulation of factors that normally control *icd-1* expression, or via some other means that globally regulates translational activity remains unclear. There must be some specificity in the translational targets of ATR-1, however, because simply elevating global rRNA production by inhibiting *ncl-1*, a negative regulator of FIB-1/fibrillarin, a nucleolar protein involved in the regulation and maturation of rRNA, is not sufficient to block the size reduction caused by *isp-1* bacterial feeding RNAi (Figure 8E,F). Collectively, our results lead to a model for how ATL-1 acts to modulate the mitochondrial threshold effect (Figure 8G).

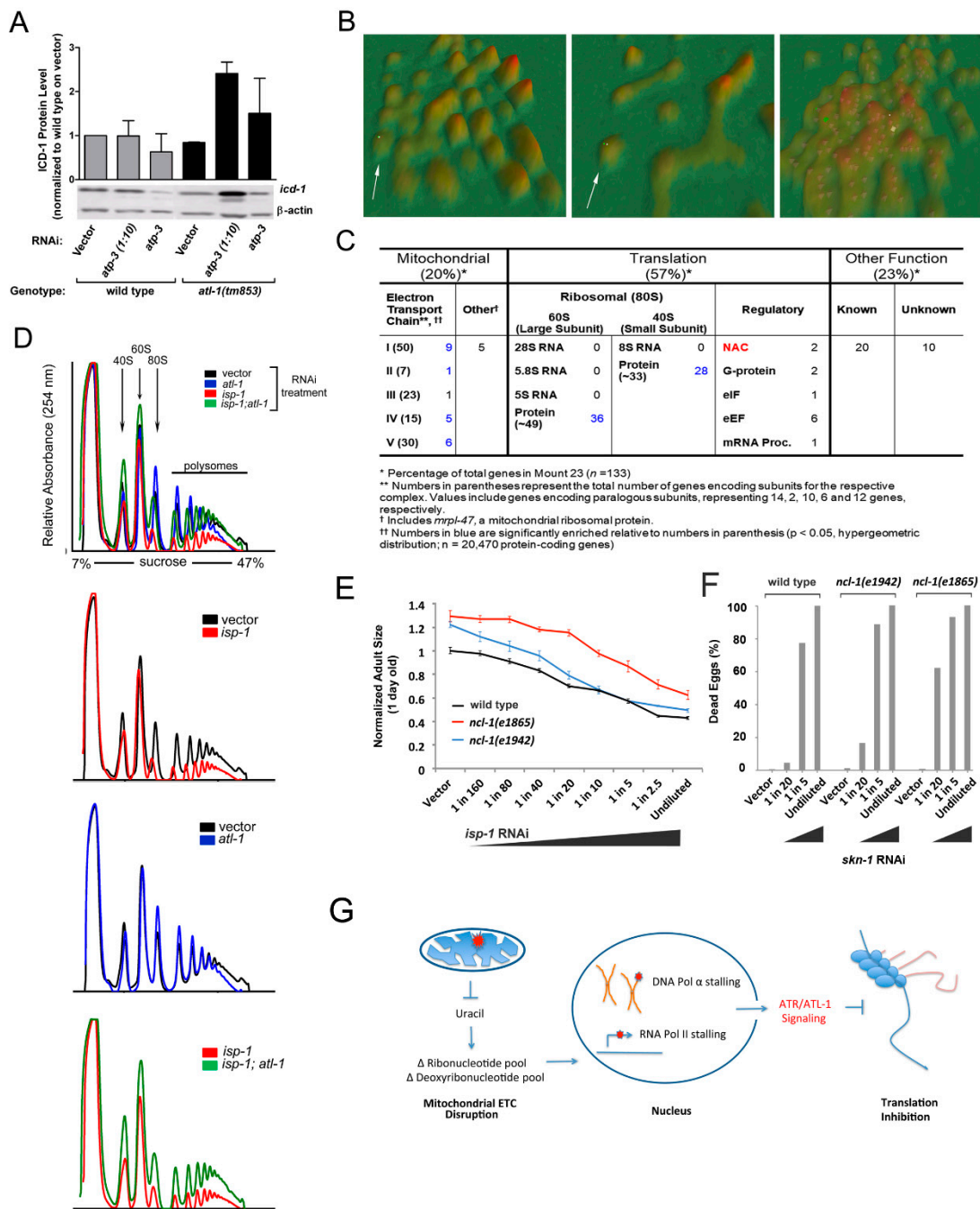


Figure 8. Knockdown of *atl-1* prevents global translation reduction caused by mitochondrial ETC disruption. (A) *Top panel:* ICD-1 protein abundance in *atl-1(tm853)* mutants relative to wild type

animals following *atp-3* knockdown ($N = 2$, bars indicate range). *Bottom panel*: Representative western blot. All worms are the unbalanced F1 progeny of parents carrying the nT1 reciprocal chromosomal translocation. (B) *C. elegans* gene co-expression terrain map generated using VxInsight [66] showing *icd-1*-containing 'Mount 23' (white arrow). Progressive zoom shots of Mount 23 are shown (left to right). The position of *icd-1* is marked by a white square. (C) 88 of 133 (66%) genes comprising Mount 23 of the *C. elegans* gene co-expression terrain map encode either mitochondrial ETC proteins or ribosomal proteins, including both α - and β -NAC (ICD-1). (D) Polysome profiling shows knockdown of *atl-1* (9/10th RNAi strength) restores the level of actively-translating ribosomes to control levels in worms grown on *isp-1* RNAi (1/10th strength). (E) *ncl-1(e1865)* and *ncl-1(e1942)* mutants do not confer resistance to the size-reducing effects of bacterial feeding RNAi targeting *isp-1* relative to wild type (N2) worms. *ncl-1* mutants are naturally larger than N2 worms. (mean \pm SEM). (F) RNAi remains efficacious in *ncl-1(e1865)* and *ncl-1(e1942)* mutants. Shown is survival following exposure to increasing doses of a lethal feeding RNAi (*skn-1*). Data from a single experiment are shown that were established simultaneously with common reagents and using 20 synchronous one-day-old adult worms per test condition. (G) Model showing how removal of ATL-1 counters loss of mitochondrial electron transport chain disruption. ETC insufficiency results in nucleotide imbalances, stalling of nucleotide polymerases, activation of ATL-1, and dampening of global translation, leading to magnification of ETC dysfunction.

4. Discussion

In this study, we discovered that the PIKK kinase ATR/ATL-1 plays a specific role in modulating the mitochondrial threshold effect of *C. elegans*. When flux through the ETC was reduced, ATL-1 was activated. We presented data suggesting that the stalling of RNA polymerase could be the trigger for ATL-1 activation. We recorded measurable reductions in many nucleotide species in adult worms, including substrates for both RNA and DNA polymerase, and we presented biochemical evidence showing RNA polymerase stalling following ETC disruption. In addition to these findings, we showed that ATL-1 paradoxically exacerbates mitochondrial dysfunction during times of mitochondrial stress. Specifically, when worms containing reduced levels of *atl-1* were challenged with ETC disruption, unlike wild type animals, these animals showed no signs of impairment in global translational output or respiratory oxygen consumption. Phenotypically, loss of *atl-1* effectively reversed a mitochondrial ETC insufficiency in *C. elegans*. The survival benefits of further dampening ETC activity following an ETC insult are not entirely clear, but dampening of mitochondrial respiratory activity in conjunction with global translational dampening might represent an effort to slow overall metabolism or to maintain stoichiometric balance between nuclear- and mitochondria-encoded ETC proteins [67].

4.1. Mode of ATL-1 Activation Following Mitochondrial ETC Disruption

In our search for signals that triggered ATL-1 activation in response to ETC disruption, we found no evidence for elevated rates of nuclear DNA mutation or strand breakage. This does not preclude the possibility that DNA damage occurred and was accurately repaired. Such damage would have escaped detection in our assays. Nonetheless, we investigated other potential mechanisms of ATL-1 activation, and, in *isp-1(qm150)* mutants, found that nucleotide pools were significantly changed. This is significant because ATR activation has been linked to changes in nucleotide pools in other model systems. Specifically, in *S. cerevisiae*, glucose starvation induces Snf1p (AMP kinase) at the mitochondrial surface following reduction of adenosine ribonucleotide energy charge. In turn, Snf1p was shown to phosphorylate Mec1p (ATR) [32]. Whether a similar mode of ATR activation functions in *C. elegans* remains unclear, but Ggc1p, the protein that initially recruits Mec1p to the yeast mitochondrial membrane under low-glucose conditions, has no worm ortholog. We pursued an alternate hypothesis for nucleotide-dependent activation of ATR in worms, namely the stalling of RNA and/or DNA polymerases.

Previously, it had been shown that blocking RNA polymerase during transcriptional elongation is sufficient to activate ATR and induce a DNA damage response (DDR) [55].

Indeed, we found evidence that DNA::RNA R-loop hybrids are increased in the presence of mitochondrial ETC disruption, which is indicative of transcriptional stalling. However, it is unclear whether all the R-loops we detected were genomic DNA (gDNA)-derived transcription intermediates. When examining samples on an agarose gel in conjunction with an antibody targeting these structures (S9.6), R-loops are expected to appear at a high molecular weight in association with the gDNA band. We clearly detected an elevated signal in this region in our *isp-1* RNAi-treated samples, consistent with our hypothesis. Moreover, we observed an additional smear of low molecular weight nucleic acids. At this point, it is unknown if these low molecular weight molecules are truly DNA::RNA hybrids or a contaminating nucleic acid. The S9.6 antibody has a five-fold higher affinity for DNA::RNA hybrids over RNA::RNA hybrids [38], so in anticipation of the latter, our samples were treated with RNase A, ruling out this possibility. One idea is that the low molecular weight DNA::RNA hybrids are derived from mtDNA fragments that have leaked from dysfunctional mitochondria. Consistent with this idea, in mouse embryonic fibroblasts, mitochondrial stress results in mtDNA leaking into the cytoplasm and initiating an immune response [68]. On the other hand, worms use a rolling circle replication method for their mtDNA, so precisely how R-loops would form in the absence of D-loop (θ) replication, as is used by mammalian cells, remains enigmatic [69]. Another idea is that the low molecular weight species we detected are cytoplasmic DNA::RNA hybrids produced by DNA polymerase α (DNA pol α). Starokadomsky and colleagues [70] showed that a small fraction of DNA pol α localizes to the cytoplasm in human cells, where it generates DNA::RNA hybrids. These molecules directly modulate production of type I interferons, and possibly exist to control the activation threshold of the innate immune response by foreign nucleic acids. In patients with X-linked reticulate pigmentary disorder (XLPDR), a primary immunodeficiency with autoinflammatory features, levels of the catalytic subunit of DNA pol α (DNA PolA1) are decreased enough to disrupt cytoplasmic DNA::RNA hybrid formation, but not enough to affect DNA replication [70]. Intriguingly, in our screen for DDR proteins that, when inhibited, reversed the small size phenotype of *atl-1(tm853); atm-1(gk186)* double mutants experiencing mitochondrial ETC stress, we identified an RNAi clone targeting DNA PolA1. Although not discussed earlier, we also isolated a second DNA pol α clone in that screen that targeted a different region of DNA PolA1, but instead resulted in synthetic lethality. This dose-dependent phenotypic response is remarkably similar to what was just discussed for humans. Obviously, more work is needed to determine the identity, provenance, and significance of the low molecular weight DNA::RNA species in worms experiencing ETC stress, and if and how they might relate to ATR activation.

4.2. Downstream Targets of ATL-1 That Modulate Mitochondrial ETC Activity

One important finding from our study is the observation that *atl-1* knockdown mitigates the effects of mitochondrial ETC dysfunction. This is an intriguing finding, as it suggests the normal cellular response to ETC disruption is ostensibly further detrimental. Two possible explanations for how the loss of *atl-1* could result in enhanced ETC function are: *atl-1* knockdown triggers active restoration of mitochondrial function, or, alternatively, *atl-1* knockdown precludes propagation of whatever negative downstream effects are normally elicited by ETC disruption. According to our data, *atl-1(tm853)* mutants contain half the amount of mtDNA as wild type worms, and have a significantly reduced abundance of nuclear-encoded ETC transcripts. These findings argue against the first hypothesis. Surprisingly, despite their shortcomings, we find that *atl-1(tm853)* mutants are still able to maintain oxygen consumption at near normal levels when confronted with ETC disruption. The precise mechanism involved is yet to be determined, but it may be as simple as *atl-1(tm853)* mutants being able to maintain the translation of a factor that enhances supercomplex formation, for example [71]. Alternatively, *atl-1(tm853)* mutants may be able to keep their cells fortified with sufficient ETC proteins to counteract any rapid turnover that is likely to occur when subunits become rate-limiting during the assembly process. Along these lines, when we examined polysome formation under conditions of ETC dysfunction, we found

that animals with functional ATL-1 had reduced polysome formation, but removal of *atl-1* restored this number back to pre-ETC disruption levels. Future studies will be aimed at determining the precise mRNA species present in these polysomes.

Another way in which *atl-1(tm853)* mutants might be able to counter ETC disruption involves the nascent protein-folding machinery. We showed that ICD-1/ β NAC, a protein that acts as a ribosome-associated chaperone, is upregulated in *atl-1* mutants upon ETC disruption. In yeast and plants, β NAC plays a role in targeting proteins to the mitochondria, and is required for efficient mitochondrial function [72–76]. β NAC was also one of the few proteins found to be specifically regulated by ATR-dependent phosphorylation in mammals [20]. The ATR-dependent phosphorylation site in mammals is not conserved in *C. elegans*; however, there are several other potential phosphorylation sites in the ICD-1 protein sequence [77]. It will be of particular interest in the future to ascertain if ATR directly regulates β NAC abundance on ribosomes to modulate translation of ETC transcripts in worms.

4.3. Mitochondrial Dysfunction in Mammals

Johnson and colleagues [78] successfully extended the survival of a mouse model of Leigh syndrome, which was deficient in *Ndufs4* of complex I, by chronic administration of the mTOR inhibitor, rapamycin. mTOR is a positive regulator of p70S6 kinase, and a negative regulator of 4E-BP, both of which work to elevate translation. At first, this seems surprising in light of our findings, suggesting global translation needs to be elevated to counter ETC dysfunction in worms. However, though acute inhibition of mTOR indeed results in a global dampening of translation, it also results in the specific translational upregulation of mitochondrial ETC components [79,80]. Moreover, it has been reported that in contrast to acute rapamycin administration, chronic rapamycin administration does not lead to reduced ribosomal activity in vivo [81]. Whether the increase in polysomes that we observed in *atl-1* animals exposed to ETC disruption represented upregulation of global mRNA translation or just a discrete subset of mRNAs only encoding ETC proteins remains to be determined.

In conclusion, we have shown that the blockade of *atl-1* effectively reverses ETC disruption in *C. elegans*. Preventing mitochondria from transitioning into their critical ETC threshold appears, quite literally, to be the difference between life and death.

Supplementary Materials: The following supporting information can be downloaded at: <https://www.mdpi.com/article/10.3390/cells11111731/s1>, Figure S1. Loss of ATL-1 desensitizes worms to mitochondrial respiratory chain stress induced by ethidium bromide. Figure S2. DNA mutation detection in *C. elegans* using β -Gal frame-shift and TUNEL assays. Figure S3. Nucleotide biosynthesis in *C. elegans* highlighting the role of the mitochondrial ETC. Figure S4. mRNA splicing remains unaltered in worms experiencing ETC disruption, both in the absence or presence of *atl-1* knockdown. Figure S5. *atl-1* knockdown does not alter retrograde response pathways normally induced by mitochondrial ETC stress. Table S1. Summary of descriptive statistics for final-round DDR RNAi screen hits (related to Figure 3). Table S2. Mean ranks of final-round DDR RNAi hits used for Kruskal–Wallis test (related to Figure 3). Table S3. Post-hoc tests for each final-round DDR RNAi hit versus vector (related to Figure 3). Table S4. List of *C. elegans* strains employed in current study. Table S5. qPCR primer list. File S1. Supplemental Methods and Supplemental Figure Legends. File S2. Mean difference ratios of all hits from DNA Damage Response (DDR) screen (related to Figure 3). File S3. Significance testing for differences in HXK2::GFP fluorescence (related to Figure 7C). References [82–92] are cited in Supplementary Materials.

Author Contributions: Conceptualization, M.B.B., N.V. and S.L.R.; methodology, M.K.C., V.L.M. and X.G.; software, S.L.R.; formal analysis, M.G., M.K.C. and S.L.R.; investigation, M.B.B., A.K., B.H., S.B. (Shylesh Bhaskaran), S.B. (Sandra Becerra), N.N., N.V. and S.L.R.; writing—original draft preparation, M.B.B. and S.L.R.; writing—review and editing, all authors.; supervision, T.E.J., B.K.K., S.L.R.; project administration, S.L.R.; funding acquisition, M.B.B., T.E.J., B.K.K., S.L.R. All authors have read and agreed to the published version of the manuscript.

Funding: Financial support was provided by the National Institutes of Health (AG-047561 (SLR), AG025207 (SLR), AG-055820 (SLR) and K12GM111726 (MBB)). Funding sources had no role in the study design, data collection and analysis, the decision to publish, or preparation of the manuscript.

Institutional Review Board Statement: Not applicable.

Informed Consent Statement: Not applicable.

Data Availability Statement: All data presented in this study are contained within the article or Supplemental Materials. Raw data files are available upon request from the corresponding author (SLR).

Acknowledgments: We thank the following people: Hidehito Kuroyanagi (Tokyo Medical and Dental University) for the splice reporters; Joel Rothman (UCSB) for the *icd-1* antibody; Alison Kell (CU, Boulder) for assistance with DDR library construction; Oxana Radetskaya (UW) for critical reading of the manuscript. Technical assistance was provided by Rebecca Lane, Carlos Galeano, Yvonne Penrod, Haley Beam, Bill Swan, and Melissa Ligon (all UT Health San Antonio). We also thank Wormbase. Some strains were provided by the *Caenorhabditis* Genetic Stock Center, which is funded by NIH Office of Research Infrastructure Programs (P40 OD010440).

Conflicts of Interest: The authors declare no conflict of interest.

Abbreviations

ATM	ataxia telangiectasia mutated
ATFS-1	activating transcription factor associated with stress
ATL-1	ataxia telangiectasia mutated-like (<i>C. elegans</i> ortholog of ATR)
ATR	ataxia telangiectasia mutated and Rad3-related
DDR	DNA damage response
DHODH	dihydroorotate dehydrogenase
DNA pol α	DNA polymerase alpha
DNA polA1	DNA polymerase alpha catalytic subunit
ETC	electron transport chain
mtDNA	mitochondrial DNA
MAPKAP	p38 MAPK-activated protein kinase
mTOR	mechanistic target of rapamycin
PIKK	phosphoinositide 3-kinase-related kinase
R-loop	DNA:RNA hybrid
RNA pol II	RNA polymerase II
TUNEL	terminal deoxynucleotidyl transferase dUTP nick end labeling

References

- Schaefer, A.M.; Taylor, R.W.; Turnbull, D.M.; Chinnery, P.F. The epidemiology of mitochondrial disorders—Past, present and future. *Biochim. Biophys. Acta (BBA)-Bioenerg.* **2004**, *1659*, 115–120. [[CrossRef](#)] [[PubMed](#)]
- Li, M.X.; Dewson, G. Mitochondria and apoptosis: Emerging concepts. *F1000Prime Rep.* **2015**, *7*, 42. [[CrossRef](#)] [[PubMed](#)]
- Liu, Y.; Samuel, B.S.; Breen, P.C.; Ruvkun, G. *Caenorhabditis elegans* pathways that surveil and defend mitochondria. *Nature* **2014**, *508*, 406–410. [[CrossRef](#)]
- Khutornenko, A.A.; Roudko, V.V.; Chernyak, B.V.; Vartapetian, A.B.; Chumakov, P.M.; Evstafieva, A.G. Pyrimidine biosynthesis links mitochondrial respiration to the p53 pathway. *Proc. Natl. Acad. Sci. USA* **2010**, *107*, 12828–12833. [[CrossRef](#)]
- Wallace, D.C. Mitochondrial DNA mutations in disease and aging. *Environ. Mol. Mutagen.* **2010**, *51*, 440–450. [[CrossRef](#)] [[PubMed](#)]
- Wallace, D.C. Mitochondria and cancer. *Nat. Rev. Cancer* **2012**, *12*, 685–698. [[CrossRef](#)]
- Lane, R.K.; Hilsabeck, T.; Rea, S.L. The role of mitochondrial dysfunction in age-related diseases. *Biochim. Biophys. Acta (BBA)-Bioenerg.* **2015**, *1847*, 1387–1400. [[CrossRef](#)] [[PubMed](#)]
- Rosignol, R.; Faustin, B.; Rocher, C.; Malgat, M.; Mazat, J.P.; Letellier, T. Mitochondrial threshold effects. *Biochem. J.* **2003**, *370*, 751–762. [[CrossRef](#)]
- Munkácsy, E.; Rea, S.L. The paradox of mitochondrial dysfunction and extended longevity. *Exp. Gerontol.* **2014**, *56*, 221–233. [[CrossRef](#)]
- Arnould, T.; Michel, S.; Renard, P. Mitochondria Retrograde Signaling and the UPR(mt): Where Are We in Mammals? *Int. J. Mol. Sci.* **2015**, *16*, 18224–18251. [[CrossRef](#)]

11. Nargund, A.M.; Pellegrino, M.W.; Fiorese, C.J.; Baker, B.M.; Haynes, C.M. Mitochondrial import efficiency of ATFS-1 regulates mitochondrial UPR activation. *Science* **2012**, *337*, 587–590. [[CrossRef](#)] [[PubMed](#)]
12. Biswas, G.; Adebajo, O.A.; Freedman, B.D.; Anandatheerthavarada, H.K.; Vijayasathy, C.; Zaidi, M.; Kotlikoff, M.; Avadhani, N.G. Retrograde Ca²⁺ signaling in C2C12 skeletal myocytes in response to mitochondrial genetic and metabolic stress: A novel mode of inter-organelle crosstalk. *EMBO J.* **1999**, *18*, 522–533. [[CrossRef](#)] [[PubMed](#)]
13. Munkacsy, E.; Khan, M.H.; Lane, R.K.; Borror, M.B.; Park, J.H.; Bokov, A.F.; Fisher, A.L.; Link, C.D.; Rea, S.L. DLK-1, SEK-3 and PMK-3 Are Required for the Life Extension Induced by Mitochondrial Bioenergetic Disruption in *C. elegans*. *PLoS Genet.* **2016**, *12*, e1006133. [[CrossRef](#)] [[PubMed](#)]
14. Heo, J.M.; Livnat-Levanon, N.; Taylor, E.B.; Jones, K.T.; Dephoure, N.; Ring, J.; Xie, J.; Brodsky, J.L.; Madeo, F.; Gygi, S.P.; et al. A stress-responsive system for mitochondrial protein degradation. *Mol. Cell* **2010**, *40*, 465–480. [[CrossRef](#)] [[PubMed](#)]
15. Jiang, P.; Jin, X.; Peng, Y.; Wang, M.; Liu, H.; Liu, X.; Zhang, Z.; Ji, Y.; Zhang, J.; Liang, M.; et al. The exome sequencing identified the mutation in YARS2 encoding the mitochondrial tyrosyl-tRNA synthetase as a nuclear modifier for the phenotypic manifestation of Leber’s hereditary optic neuropathy-associated mitochondrial DNA mutation. *Hum. Mol. Genet.* **2016**, *25*, 584–596. [[CrossRef](#)] [[PubMed](#)]
16. Huyen, Y.; Jeffrey, P.D.; Derry, W.B.; Rothman, J.H.; Pavletich, N.P.; Stavridi, E.S.; Halazonetis, T.D. Structural Differences in the DNA Binding Domains of Human p53 and Its *C. elegans* Ortholog Cep-1. *Structure* **2004**, *12*, 1237–1243. [[CrossRef](#)]
17. Ventura, N.; Rea, S.L.; Schiavi, A.; Torgovnick, A.; Testi, R.; Johnson, T.E. p53/CEP-1 increases or decreases lifespan, depending on level of mitochondrial bioenergetic stress. *Aging Cell* **2009**, *8*, 380–393. [[CrossRef](#)]
18. Schiavi, A.; Torgovnick, A.; Kell, A.; Megalou, E.; Castelein, N.; Guccini, I.; Marzocchella, L.; Gelino, S.; Hansen, M.; Malisan, F.; et al. Autophagy induction extends lifespan and reduces lipid content in response to frataxin silencing in *C. elegans*. *Exp. Gerontol.* **2013**, *48*, 191–201. [[CrossRef](#)]
19. Lovejoy, C.A.; Cortez, D. Common mechanisms of PIKK regulation. *DNA Repair* **2009**, *8*, 1004–1008. [[CrossRef](#)]
20. Matsuoka, S.; Ballif, B.A.; Smogorzewska, A.; McDonald, E.R., III; Hurov, K.E.; Luo, J.; Bakalarski, C.E.; Zhao, Z.; Solimini, N.; Lerenthal, Y.; et al. ATM and ATR Substrate Analysis Reveals Extensive Protein Networks Responsive to DNA Damage. *Science* **2007**, *316*, 1160–1166. [[CrossRef](#)]
21. Marechal, A.; Zou, L. DNA damage sensing by the ATM and ATR kinases. *Cold Spring Harb. Perspect. Biol.* **2013**, *5*, a012716. [[CrossRef](#)] [[PubMed](#)]
22. Vousden, K.H.; Lane, D.P. p53 in health and disease. *Nat. Rev. Mol. Cell Biol.* **2007**, *8*, 275–283. [[CrossRef](#)] [[PubMed](#)]
23. Yang, D.Q.; Kastan, M.B. Participation of ATM in insulin signalling through phosphorylation of eIF-4E-binding protein 1. *Nat. Cell Biol.* **2000**, *2*, 893–898. [[CrossRef](#)] [[PubMed](#)]
24. Schneider, J.G.; Finck, B.N.; Ren, J.; Standley, K.N.; Takagi, M.; Maclean, K.H.; Bernal-Mizrachi, C.; Muslin, A.J.; Kastan, M.B.; Semenkovich, C.F. ATM-dependent suppression of stress signaling reduces vascular disease in metabolic syndrome. *Cell Metab.* **2006**, *4*, 377–389. [[CrossRef](#)]
25. Cosentino, C.; Grieco, D.; Costanzo, V. ATM activates the pentose phosphate pathway promoting anti-oxidant defence and DNA repair. *EMBO J.* **2011**, *30*, 546–555. [[CrossRef](#)]
26. Schroeder, E.A.; Raimundo, N.; Shadel, G.S. Epigenetic silencing mediates mitochondria stress-induced longevity. *Cell Metab.* **2013**, *17*, 954–964. [[CrossRef](#)]
27. Fang, E.F.; Bohr, V.A. NAD⁺: The convergence of DNA repair and mitophagy. *Autophagy* **2017**, *13*, 442–443. [[CrossRef](#)]
28. Chioldi, I.; Minoda, A.; Colmenares, S.U.; Polyzos, A.; Costes, S.V.; Karpen, G.H. Double-strand breaks in heterochromatin move outside of a dynamic HP1a domain to complete recombinational repair. *Cell* **2011**, *144*, 732–744. [[CrossRef](#)]
29. Gupta, A.; Sharma, S.; Reichenbach, P.; Marjavaara, L.; Nilsson, A.K.; Lingner, J.; Chabes, A.; Rothstein, R.; Chang, M. Telomere length homeostasis responds to changes in intracellular dNTP pools. *Genetics* **2013**, *193*, 1095–1105. [[CrossRef](#)]
30. Kumar, A.; Mazzanti, M.; Mistrik, M.; Kosar, M.; Beznoussenko, G.V.; Mironov, A.A.; Garre, M.; Parazzoli, D.; Shivashankar, G.V.; Scita, G.; et al. ATR mediates a checkpoint at the nuclear envelope in response to mechanical stress. *Cell* **2014**, *158*, 633–646. [[CrossRef](#)]
31. Hilton, B.A.; Li, Z.; Musich, P.R.; Wang, H.; Cartwright, B.M.; Serrano, M.; Zhou, X.Z.; Lu, K.P.; Zou, Y. ATR Plays a Direct Antiapoptotic Role at Mitochondria, which Is Regulated by Prolyl Isomerase Pin1. *Mol. Cell* **2015**, *60*, 35–46. [[CrossRef](#)] [[PubMed](#)]
32. Yi, C.; Tong, J.; Lu, P.; Wang, Y.; Zhang, J.; Sun, C.; Yuan, K.; Xue, R.; Zou, B.; Li, N.; et al. Formation of a Snf1-Mec1-Atg1 Module on Mitochondria Governs Energy Deprivation-Induced Autophagy by Regulating Mitochondrial Respiration. *Dev. Cell* **2017**, *41*, 59–71.e4. [[CrossRef](#)] [[PubMed](#)]
33. Wood, W.B. (Ed.) *The Nematode Caenorhabditis elegans*; Cold Spring Harbor Laboratory: New York, NY, USA, 1988; p. 667.
34. Timmons, L.; Fire, A. Specific interference by ingested dsRNA. *Nature* **1998**, *395*, 854. [[CrossRef](#)] [[PubMed](#)]
35. Hoogewijs, D.; Houthoofd, K.; Matthijsens, F.; Vandesompele, J.; Vanfleteren, J.R. Selection and validation of a set of reliable reference genes for quantitative sod gene expression analysis in *C. elegans*. *BMC Mol. Biol.* **2008**, *9*, 9. [[CrossRef](#)]
36. Sugimoto, T.; Mori, C.; Takanami, T.; Sasagawa, Y.; Saito, R.; Ichiishi, E.; Higashitani, A. *Caenorhabditis elegans* par2.1/mtssb-1 is essential for mitochondrial DNA replication and its defect causes comprehensive transcriptional alterations including a hypoxia response. *Exp. Cell Res.* **2008**, *314*, 103–114. [[CrossRef](#)]
37. Rooney, J.P.; Ryde, I.T.; Sanders, L.H.; Howlett, E.H.; Colton, M.D.; Germ, K.E.; Mayer, G.D.; Greenamyre, J.T.; Meyer, J.N. PCR based determination of mitochondrial DNA copy number in multiple species. *Methods Mol. Biol.* **2015**, *1241*, 23–38. [[CrossRef](#)]

38. Zhang, Z.Z.; Pannunzio, N.R.; Hsieh, C.L.; Yu, K.; Lieber, M.R. Complexities due to single-stranded RNA during antibody detection of genomic RNA:DNA hybrids. *BMC Res. Notes* **2015**, *8*, 127. [[CrossRef](#)]
39. Kuroyanagi, H.; Watanabe, Y.; Suzuki, Y.; Hagiwara, M. Position-dependent and neuron-specific splicing regulation by the CELF family RNA-binding protein UNC-75 in *Caenorhabditis elegans*. *Nucleic Acids Res.* **2013**, *41*, 4015–4025. [[CrossRef](#)]
40. Kuroyanagi, H.; Ohno, G.; Sakane, H.; Maruoka, H.; Hagiwara, M. Visualization and genetic analysis of alternative splicing regulation in vivo using fluorescence reporters in transgenic *Caenorhabditis elegans*. *Nat. Protoc.* **2010**, *5*, 1495–1517. [[CrossRef](#)]
41. Luz, A.L.; Rooney, J.P.; Kubik, L.L.; Gonzalez, C.P.; Song, D.H.; Meyer, J.N. Mitochondrial Morphology and Fundamental Parameters of the Mitochondrial Respiratory Chain Are Altered in *Caenorhabditis elegans* Strains Deficient in Mitochondrial Dynamics and Homeostasis Processes. *PLoS ONE* **2015**, *10*, e0130940. [[CrossRef](#)]
42. Steffen, K.K.; MacKay, V.L.; Kerr, E.O.; Tsuchiya, M.; Hu, D.; Fox, L.A.; Dang, N.; Johnston, E.D.; Oakes, J.A.; Tchao, B.N.; et al. Yeast life span extension by depletion of 60s ribosomal subunits is mediated by Gcn4. *Cell* **2008**, *133*, 292–302. [[CrossRef](#)] [[PubMed](#)]
43. Torgovnick, A.; Schiavi, A.; Shaik, A.; Kassahun, H.; Maglioni, S.; Rea, S.L.; Johnson, T.E.; Reinhardt, H.C.; Honnen, S.; Schumacher, B.; et al. BRCA1 and BARD1 mediate apoptotic resistance but not longevity upon mitochondrial stress in *Caenorhabditis elegans*. *EMBO Rep.* **2018**, *19*, e45856. [[CrossRef](#)] [[PubMed](#)]
44. Rea, S.L.; Ventura, N.; Johnson, T.E. Relationship between mitochondrial electron transport chain dysfunction, development, and life extension in *Caenorhabditis elegans*. *PLoS Biol.* **2007**, *5*, e259. [[CrossRef](#)] [[PubMed](#)]
45. Satsuka, A.; Mehta, K.; Laimins, L. p38MAPK and MK2 pathways are important for the differentiation-dependent human papillomavirus life cycle. *J. Virol.* **2015**, *89*, 1919–1924. [[CrossRef](#)] [[PubMed](#)]
46. Reinhardt, H.C.; Aslanian, A.S.; Lees, J.A.; Yaffe, M.B. p53-Deficient Cells Rely on ATM- and ATR-Mediated Checkpoint Signaling through the p38MAPK/MK2 Pathway for Survival after DNA Damage. *Cancer Cell* **2007**, *11*, 175–189. [[CrossRef](#)] [[PubMed](#)]
47. Manke, I.A.; Nguyen, A.; Lim, D.; Stewart, M.Q.; Elia, A.E.; Yaffe, M.B. MAPKAP kinase-2 is a cell cycle checkpoint kinase that regulates the G2/M transition and S phase progression in response to UV irradiation. *Mol. Cell* **2005**, *17*, 37–48. [[CrossRef](#)] [[PubMed](#)]
48. Garcia-Muse, T.; Boulton, S.J. Distinct modes of ATR activation after replication stress and DNA double-strand breaks in *Caenorhabditis elegans*. *EMBO J.* **2005**, *24*, 4345–4355. [[CrossRef](#)]
49. Dmitrieva, N.I.; Celeste, A.; Nussenzweig, A.; Burg, M.B. Ku86 preserves chromatin integrity in cells adapted to high NaCl. *Proc. Natl. Acad. Sci. USA* **2005**, *102*, 10730–10735. [[CrossRef](#)]
50. Desler, C.; Lykke, A.; Rasmussen, L.J. The effect of mitochondrial dysfunction on cytosolic nucleotide metabolism. *J. Nucleic Acids* **2010**, *2010*, 701518. [[CrossRef](#)]
51. Kuchta, R.D.; Stengel, G. Mechanism and evolution of DNA primases. *Biochim. Biophys. Acta (BBA)-Bioenerg.* **2010**, *1804*, 1180–1189. [[CrossRef](#)]
52. Guillian, T.A.; Keen, B.A.; Brissett, N.C.; Doherty, A.J. Primase-polymerases are a functionally diverse superfamily of replication and repair enzymes. *Nucleic Acids Res.* **2015**, *43*, 6651–6664. [[CrossRef](#)]
53. Zou, L.; Elledge, S.J. Sensing DNA damage through ATRIP recognition of RPA-ssDNA complexes. *Science* **2003**, *300*, 1542–1548. [[CrossRef](#)] [[PubMed](#)]
54. Tsang, W.Y.; Lemire, B.D. Mitochondrial Genome Content Is Regulated during Nematode Development. *Biochem. Biophys. Res. Commun.* **2002**, *291*, 8–16. [[CrossRef](#)] [[PubMed](#)]
55. Derheimer, F.A.; O'Hagan, H.M.; Krueger, H.M.; Hanasoge, S.; Paulsen, M.T.; Ljungman, M. RPA and ATR link transcriptional stress to p53. *Proc. Natl. Acad. Sci. USA* **2007**, *104*, 12778–12783. [[CrossRef](#)] [[PubMed](#)]
56. Hamperl, S.; Cimprich, K.A. The contribution of co-transcriptional RNA:DNA hybrid structures to DNA damage and genome instability. *DNA Repair* **2014**, *19*, 84–94. [[CrossRef](#)] [[PubMed](#)]
57. Sollier, J.; Cimprich, K.A. Breaking bad: R-loops and genome integrity. *Trends Cell Biol.* **2015**, *25*, 514–522. [[CrossRef](#)]
58. Proudfoot, N.J.; Furger, A.; Dye, M.J. Integrating mRNA processing with transcription. *Cell* **2002**, *108*, 501–512. [[CrossRef](#)]
59. Heintz, C.; Doktor, T.K.; Lanjuin, A.; Escoubas, C.; Zhang, Y.; Weir, H.J.; Dutta, S.; Silva-Garcia, C.G.; Bruun, G.H.; Morantte, I.; et al. Splicing factor 1 modulates dietary restriction and TORC1 pathway longevity in *C. elegans*. *Nature* **2017**, *541*, 102–106. [[CrossRef](#)]
60. Kuroyanagi, H.; Kobayashi, T.; Mitani, S.; Hagiwara, M. Transgenic alternative-splicing reporters reveal tissue-specific expression profiles and regulation mechanisms in vivo. *Nat. Methods* **2006**, *3*, 909–915. [[CrossRef](#)]
61. Ventura, N.; Rea, S.L. *Caenorhabditis elegans* mitochondrial mutants as an investigative tool to study human neurodegenerative diseases associated with mitochondrial dysfunction. *Biotechnol. J.* **2007**, *2*, 584–595. [[CrossRef](#)]
62. Mori, C.; Takanami, T.; Higashitani, A. Maintenance of mitochondrial DNA by the *Caenorhabditis elegans* ATR checkpoint protein ATL-1. *Genetics* **2008**, *180*, 681–686. [[CrossRef](#)]
63. Henderson, S.T.; Bonafe, M.; Johnson, T.E. daf-16 protects the nematode *Caenorhabditis elegans* during food deprivation. *J. Gerontol. Ser. A Biol. Sci. Med. Sci.* **2006**, *61*, 444–460. [[CrossRef](#)] [[PubMed](#)]
64. Bloss, T.A.; Witze, E.S.; Rothman, J.H. Suppression of CED-3-independent apoptosis by mitochondrial β NAC in *Caenorhabditis elegans*. *Nature* **2003**, *424*, 1066–1071. [[CrossRef](#)] [[PubMed](#)]
65. Arsenovic, P.T.; Maldonado, A.T.; Colleluori, V.D.; Bloss, T.A. Depletion of the *C. elegans* NAC engages the unfolded protein response, resulting in increased chaperone expression and apoptosis. *PLoS ONE* **2012**, *7*, e44038. [[CrossRef](#)] [[PubMed](#)]

66. Kim, S.K.; Lund, J.; Kiraly, M.; Duke, K.; Jiang, M.; Stuart, J.M.; Eizinger, A.; Wylie, B.N.; Davidson, G.S. A gene expression map for *Caenorhabditis elegans*. *Science* **2001**, *293*, 2087–2092. [[CrossRef](#)]
67. Houtkooper, R.H.; Mouchiroud, L.; Ryu, D.; Moullan, N.; Katsyuba, E.; Knott, G.; Williams, R.W.; Auwerx, J. Mitonuclear protein imbalance as a conserved longevity mechanism. *Nature* **2013**, *497*, 451–457. [[CrossRef](#)]
68. West, A.P.; Khoury-Hanold, W.; Staron, M.; Tal, M.C.; Pineda, C.M.; Lang, S.M.; Bestwick, M.; Duguay, B.A.; Raimundo, N.; MacDuff, D.A.; et al. Mitochondrial DNA stress primes the antiviral innate immune response. *Nature* **2015**, *520*, 553–557. [[CrossRef](#)]
69. Lewis, S.C.; Joers, P.; Willcox, S.; Griffith, J.D.; Jacobs, H.T.; Hyman, B.C. A rolling circle replication mechanism produces multimeric lariats of mitochondrial DNA in *Caenorhabditis elegans*. *PLoS Genet.* **2015**, *11*, e1004985. [[CrossRef](#)]
70. Starokadomskyy, P.; Gemelli, T.; Rios, J.J.; Xing, C.; Wang, R.C.; Li, H.; Pokatayev, V.; Dozmorov, I.; Khan, S.; Miyata, N.; et al. DNA polymerase- α regulates the activation of type I interferons through cytosolic RNA:DNA synthesis. *Nat. Immunol.* **2016**, *17*, 495–504. [[CrossRef](#)]
71. Milenkovic, D.; Blaza, J.N.; Larsson, N.G.; Hirst, J. The Enigma of the Respiratory Chain Supercomplex. *Cell Metab.* **2017**, *25*, 765–776. [[CrossRef](#)]
72. George, R.; Beddoe, T.; Landl, K.; Lithgow, T. The yeast nascent polypeptide-associated complex initiates protein targeting to mitochondria in vivo. *Proc. Natl. Acad. Sci. USA* **1998**, *95*, 2296–2301. [[CrossRef](#)] [[PubMed](#)]
73. George, R.; Walsh, P.; Beddoe, T.; Lithgow, T. The nascent polypeptide-associated complex (NAC) promotes interaction of ribosomes with the mitochondrial surface in vivo. *FEBS Lett.* **2002**, *516*, 213–216. [[CrossRef](#)]
74. Yogev, O.; Karniely, S.; Pines, O. Translation-coupled translocation of yeast fumarase into mitochondria in vivo. *J. Biol. Chem.* **2007**, *282*, 29222–29229. [[CrossRef](#)] [[PubMed](#)]
75. Yang, K.-S.; Kim, H.-S.; Jin, U.-H.; Lee, S.; Park, J.-A.; Lim, Y.; Pai, H.-S. Silencing of NbBTF3 results in developmental defects and disturbed gene expression in chloroplasts and mitochondria of higher plants. *Planta* **2007**, *225*, 1459–1469. [[CrossRef](#)]
76. del Alamo, M.; Hogan, D.J.; Pechmann, S.; Albanese, V.; Brown, P.O.; Frydman, J. Defining the specificity of cotranslationally acting chaperones by systematic analysis of mRNAs associated with ribosome-nascent chain complexes. *PLoS Biol.* **2011**, *9*, e1001100. [[CrossRef](#)]
77. Amanchy, R.; Periaswamy, B.; Mathivanan, S.; Reddy, R.; Tattikota, S.G.; Pandey, A. A curated compendium of phosphorylation motifs. *Nat. Biotechnol.* **2007**, *25*, 285–286. [[CrossRef](#)]
78. Johnson, S.C.; Yanos, M.E.; Kayser, E.B.; Quintana, A.; Sangesland, M.; Castanza, A.; Uhde, L.; Hui, J.; Wall, V.Z.; Gagnidze, A.; et al. mTOR inhibition alleviates mitochondrial disease in a mouse model of Leigh syndrome. *Science* **2013**, *342*, 1524–1528. [[CrossRef](#)]
79. Zid, B.M.; Rogers, A.N.; Katewa, S.D.; Vargas, M.A.; Kolipinski, M.C.; Lu, T.A.; Benzer, S.; Kapahi, P. 4E-BP extends lifespan upon dietary restriction by enhancing mitochondrial activity in *Drosophila*. *Cell* **2009**, *139*, 149–160. [[CrossRef](#)]
80. Bonawitz, N.D.; Chatenay-Lapointe, M.; Pan, Y.; Shadel, G.S. Reduced TOR Signaling Extends Chronological Life Span via Increased Respiration and Upregulation of Mitochondrial Gene Expression. *Cell Metab.* **2007**, *5*, 265–277. [[CrossRef](#)]
81. Garelick, M.G.; Mackay, V.L.; Yanagida, A.; Academia, E.C.; Schreiber, K.H.; Ladiges, W.C.; Kennedy, B.K. Chronic rapamycin treatment or lack of S6K1 does not reduce ribosome activity in vivo. *Cell Cycle* **2013**, *12*, 2493–2504. [[CrossRef](#)]
82. Jones, M.R.; Huang, J.C.; Chua, S.Y.; Baillie, D.L.; Rose, A.M. The *atm-1* gene is required for genome stability in *Caenorhabditis elegans*. *Mol. Genet. Genom.* **2012**, *287*, 325–335. [[CrossRef](#)]
83. Kamath, R.S.; Ahringer, J. Genome-wide RNAi screening in *Caenorhabditis elegans*. *Methods* **2003**, *30*, 313–321. [[CrossRef](#)]
84. Butler, J.A.; Ventura, N.; Johnson, T.E.; Rea, S.L. Long-lived mitochondrial (Mit) mutants of *Caenorhabditis elegans* utilize a novel metabolism. *FASEB J.* **2010**, *24*, 4977–4988. [[CrossRef](#)] [[PubMed](#)]
85. Schneider, C.A.; Rasband, W.S.; Eliceiri, K.W. NIH Image to ImageJ: 25 years of image analysis. *Nat. Methods* **2012**, *9*, 671–675. [[CrossRef](#)] [[PubMed](#)]
86. Pothof, J.; van Haaften, G.; Thijssen, K.; Kamath, R.S.; Fraser, A.G.; Ahringer, J.; Plasterk, R.H.; Tijsterman, M. Identification of genes that protect the *C. elegans* genome against mutations by genome-wide RNAi. *Genes Dev.* **2003**, *17*, 443–448. [[CrossRef](#)]
87. Wu, Y.-C.; Stanfield, G.M.; Horvitz, H.R. NUC-1, a *Caenorhabditis elegans* DNase II homolog, functions in an intermediate step of DNA degradation during apoptosis. *Genes Dev.* **2000**, *14*, 536–548. [[CrossRef](#)] [[PubMed](#)]
88. Bhaskaran, S.; Butler, J.A.; Becerra, S.; Fassio, V.; Girotti, M.; Rea, S.L. Breaking *Caenorhabditis elegans* the easy way using the Balch homogenizer: An old tool for a new application. *Anal. Biochem.* **2011**, *413*, 123–132. [[CrossRef](#)]
89. Huang, D.; Zhang, Y.; Chen, X. Analysis of intracellular nucleoside triphosphate levels in normal and tumor cell lines by high-performance liquid chromatography. *J. Chromatogr. B Anal. Technol. Biomed. Life Sci.* **2003**, *784*, 101–109. [[CrossRef](#)]
90. Hoaglin, D.C.; Mosteller, F.; Tukey, J.W. *Understanding Robust and Exploratory Data Analysis*; Wiley: New York, NY, USA, 1983.
91. Dupont, W.D.; Plummer, W.D., Jr. Power and sample size calculations. A review and computer program. *Control. Clin. Trials* **1990**, *11*, 116–128. [[CrossRef](#)]
92. Dupont, W.D.; Plummer, W.D., Jr. Power and sample size calculations for studies involving linear regression. *Control. Clin. Trials* **1998**, *19*, 589–601. [[CrossRef](#)]